

University of Alberta

**A MULTI-SPECTRAL DECIMATION SCHEME FOR  
TURBULENCE SIMULATIONS**

by

Malcolm Ian William Roberts

A thesis submitted to the Faculty of Graduate Studies and Research  
in partial fulfillment of the requirements for the degree of

**Masters of Science**

in

**Applied Mathematics**

Department of Mathematical and Statistical Sciences

© Malcolm Ian William Roberts

Fall, 2006

Edmonton, Alberta

Permission is hereby granted to the University of Alberta Libraries to reproduce single

copies of this thesis and to lend or sell such copies for private, scholarly, or scientific research purposes only. Where the thesis is converted to, or otherwise made available in digital form, the University of Alberta will advise potential users of the thesis of these terms.

The author reserves all other publication and other rights in association with the copyright in the thesis and, except as herein before provided, neither the thesis nor any substantial portion thereof may be printed or otherwise reproduced in any material form whatsoever without the author's prior written permission.

## Examining Committee

Dr. John Bowman

Dr. Bryant Moodie (Chair)

Dr. Moritz Heimpel (Physics)

## Abstract

Shell models of the Gledzer–Ohkitani–Yamada (GOY) type can provide an excellent testbed for new ideas and methods for two- and three-dimensional turbulence. We review some results for Navier–Stokes turbulence and compare with results for shell models. We introduce a *multi-spectral* decimation scheme for high-Reynolds number turbulence simulations.

The nonlinear coupling coefficients on the coarse grid are calculated with a modification of the method of spectral reduction [Bowman, Shadwick, and Morrison, *Phys. Rev. Lett.* **83**, 5491 (1999)]. This decimation scheme exploits the continuity of moments of the underlying probability distribution function to replace neighbouring shells by a reduced number of representative shells with enhanced couplings. The projection and prolongation operators between the grids are designed to conserve energy.

We demonstrate how this multi-spectral scheme might be used to derive a reliable dynamic subgrid model for turbulence.

## Acknowledgements

First and foremost, I thank my supervisor, Dr. John Bowman, for the tremendous support he has offered me during my undergraduate studies and throughout my graduate program. His skill and dedication have been of great value, and he has brought insight into problems that might otherwise still be unclear. I give my gratitude to Dr. Bruno Eckhardt for both his part in the application of the method of spectral reduction to the GOY shell model, which was instrumental to my work, and advice given in the early stages of my research.

My defense committee, composed of Drs. Bryant Moodie and Moritz Heimpel, performed their task admirably, and their questions about our approach to the problem of simulating turbulence were both insightful and thought provoking. I also thank Remkes Kooistra for his effort (and honest excitement!) in proof-reading my dissertation. The study of turbulence is far from his area of expertise, and his outsider perspective was of great value.

Finally, I thank my friends and family for their support and encouragement during this busy time. I was heartened to see so many friends at my practice defense. I would particularly like to thank Micah Cooper for her love and understanding when I was continually at my computer and too injured to be able to fetch my own scotch.

Our work made use of the infrastructure and resources of the Academic Information and Communication Technologies at the University of Alberta.

# Table of Contents

<b>1</b>	<b>Introduction</b>	<b>1</b>
1.A	Navier–Stokes Turbulence . . . . .	2
1.A.1	Reynolds number and scale independence . . . . .	5
1.A.2	Turbulence in lower dimensions . . . . .	6
1.B	Shell models of turbulence . . . . .	8
1.B.1	DN model . . . . .	9
1.B.2	GOY model . . . . .	12
1.B.3	Sabra model . . . . .	16
<b>2</b>	<b>Kolmogorov Theory</b>	<b>18</b>
2.A	Application to two-dimensional turbulence . . . . .	24
2.B	Application to shell models . . . . .	28
2.C	Final comments on Kolmogorov’s results. . . . .	29
<b>3</b>	<b>Equipartition</b>	<b>34</b>
<b>4</b>	<b>Spectral Reduction</b>	<b>41</b>
4.A	Spectral reduction of Navier–Stokes turbulence . . . . .	42
4.B	Spectral reduction of shell model turbulence . . . . .	45

<b>5</b>	<b>The Multi-Spectral Method</b>	<b>51</b>
5.A	Other approximations . . . . .	52
5.B	The time-scale disparity . . . . .	54
5.C	The multi-spectral method . . . . .	54
5.D	Projection and prolongation . . . . .	58
5.D.1	Symmetric advancement . . . . .	59
5.D.2	Sequential advancement . . . . .	61
5.D.3	Phase propagation . . . . .	63
5.E	Application of spectral reduction . . . . .	65
5.F	Extension to many grids . . . . .	67
5.G	Properties of the multi-spectral method . . . . .	67
<b>6</b>	<b>Simulations and Results</b>	<b>70</b>
6.A	Inviscid turbulence . . . . .	70
6.B	Forced-dissipative turbulence . . . . .	73
6.C	Simulations with several grids . . . . .	76
<b>7</b>	<b>Conclusions</b>	<b>79</b>
7.A	Future work . . . . .	79
7.B	Applications . . . . .	81
	<b>Bibliography</b>	<b>82</b>

# List of Figures

1.1	Comparison of the logarithmic slopes of the energy and flux spectra for the GOY model. . . . .	16
2.1	Fjortoft diagram. . . . .	25
2.2	The 2D Navier–Stokes energy spectrum at intermediate times.	28
2.3	The 2D Navier–Stokes energy spectrum at late times. . . . .	29
2.4	A comparison of structure-function exponents $\zeta_p$ , $p = 2, \dots, 6$ (bottom to top) for the GOY model with experimental results.	30
2.5	Comparison of DN, GOY, and Sabra turbulence. . . . .	31
2.6	Logarithmic slopes for DN, GOY, Sabra turbulence. . . . .	32
3.1	Equipartition energy spectrum of two-dimensional Navier–Stokes turbulence. . . . .	39
3.2	Equipartition energy spectrum of “3D” GOY turbulence. . . . .	39
3.3	Equipartition energy spectrum of DN turbulence. . . . .	40
4.1	Polar wavenumber bin geometry. . . . .	44
4.2	Spectral reduction of the GOY model showing emergence of nearest-neighbour interactions. . . . .	47
4.3	Energy spectra computed with interpolated spectral reduction.	49

5.1	Relaxation time to equipartition for the GOY model. . . . .	55
5.2	Arrangement of grids for the multi-spectral method, showing interactions for a general shell model. . . . .	56
5.3	Arrangement of grids for the multi-spectral method, showing non-redundant interactions for a general shell model. . . . .	57
5.4	The multi-spectrum grid for the DN model showing all non-redundant interactions. . . . .	58
5.5	Diagram of symmetric multi-spectral method. . . . .	59
5.6	Diagram of sequential multi-spectral method. . . . .	62
5.7	Sequential time advancement with many grids. . . . .	67
5.8	The ratio of the number of modes in a spectrally reduced system to the number of modes in the original system. . . . .	69
6.1	$E(k)$ vs. $k$ for inviscid unforced turbulence with two grids and source transfer. . . . .	71
6.2	Energy vs. time for inviscid unforced turbulence with two grids and source transfer. . . . .	71
6.3	$E(k)$ vs. $k$ for inviscid unforced turbulence with two grids with projection/prolongation. . . . .	72
6.4	$E(k)$ vs. $k$ for forced-dissipative DN turbulence showing the effect of phase communication. . . . .	74
6.5	$E(k)$ vs. $k$ for forced-dissipative DN turbulence showing the effect of assumptions of adjacent-mode correlation given by (6.1), (6.2), and (6.3). . . . .	75
6.6	Multi-spectral simulations of inviscid turbulence with one, two, three, or four grids. . . . .	76

6.7	Multi-spectral simulation of forced-dissipative turbulence with two grids. . . . .	77
6.8	Multi-spectral simulation of forced-dissipative turbulence with three grids. . . . .	77
6.9	Multi-spectral simulation of forced-dissipative turbulence with four grids. . . . .	78
6.10	Multi-spectral simulation of forced-dissipative turbulence with five grids. . . . .	78

# Chapter 1

## Introduction

*In which we introduce our goal and the models under consideration.*

The Navier–Stokes equation approximates the motion of many turbulent systems that are of practical and scientific interest. This equation is simply written, but exact solutions have eluded the scientific community for over a century. In the face of such failure, the advent of powerful computer systems has given hope that we may be able to predict the behaviour of turbulent systems numerically. Unfortunately, highly turbulent systems, such as the Earth’s atmosphere, have too many spatial and temporal scales to be solved on current computer systems, and computers will not be powerful enough to address this problem directly for the foreseeable future. The goal of this work is to develop a *multi-spectral method* that affords a dramatic reduction of the computational cost of numerical approximations of turbulence. We demonstrate the method for a shell model that mimics many properties of the Navier–Stokes equation.

## 1.A Navier–Stokes Turbulence

Turbulence can be described by the Navier–Stokes equation (e.g. Frisch [1995]),

$$\frac{\partial}{\partial t} \mathbf{u} + \mathbf{u} \cdot \nabla \mathbf{u} = -\frac{1}{\rho} \nabla P + \nu \nabla^2 \mathbf{u} + \mathbf{F}. \quad (1.1)$$

Here  $\partial/\partial t$  is the (laboratory frame) *Eulerian derivative*,  $\mathbf{u} = \mathbf{u}(\mathbf{x}, t)$  the Eulerian velocity field for the fluid,  $\rho$  the fluid density,  $P$  the pressure,  $\nu$  the kinematic viscosity, and  $\mathbf{F}$  an external stirring force. The left-hand side of (1.1) is just the *Lagrangian derivative* of the velocity field:

$$\begin{aligned} \frac{d}{dt} \mathbf{u}(\mathbf{x}(t), t) &= \frac{\partial}{\partial t} \mathbf{u}(\mathbf{x}, t) + \mathbf{x}'(t) \cdot \nabla \mathbf{u}(\mathbf{x}(t), t) \\ &= \frac{\partial}{\partial t} \mathbf{u}(\mathbf{x}, t) + \mathbf{u}(\mathbf{x}(t), t) \cdot \nabla \mathbf{u}(\mathbf{x}(t), t), \end{aligned} \quad (1.2)$$

which is the rate of change of the velocity in the frame moving with the fluid. From this viewpoint, the right-hand side of (1.1) is the acceleration that a parcel of fluid would experience due to the pressure field, viscous dissipation, and external forces on the fluid.

We would like to deal with a closed system, wherein mass is conserved everywhere. This is guaranteed by the *continuity equation*,

$$\frac{d\rho}{dt} + \rho \nabla \cdot \mathbf{u} = 0. \quad (1.3)$$

When the fluid is also *incompressible*, i.e.

$$\frac{d\rho}{dt} = \frac{\partial \rho}{\partial t} + \mathbf{u} \cdot \nabla \rho = 0, \quad (1.4)$$

the velocity field has the property that  $\nabla \cdot \mathbf{u} = 0$  everywhere. This condition is implicit in the formulation of the Navier–Stokes equation in (1.1) and allows one to calculate the pressure via the velocity. The incompressibility condition is a very good approximation except under certain circumstances, e.g. during shock formation. If the initial conditions are such that  $\nabla \rho = \mathbf{0}$ , then the incompressibility condition implies that  $\partial \rho / \partial t = 0$ , and  $\nabla \rho = \mathbf{0}$  at all later times. Thus, without loss of generality, we normalise  $\rho$ , so that  $\rho \equiv 1$ . This convention is used through the remainder of this dissertation.

In the absence of the dissipative and forcing terms  $\nu \nabla^2 \mathbf{u}$  and  $\mathbf{F}$ , the Navier–Stokes equation exhibits various symmetries [Frisch 1995], and by *Noether's theorem* (e.g. Bohr *et al.* [1998]), corresponding conserved quantities. Exactly what these symmetries and conserved quantities are depends on the dimension. Given periodic or zero boundary conditions, the energy  $E \doteq \frac{1}{2} \int \mathbf{u}^2 d\mathbf{x}$  ( $\doteq$  indicates a definition) is conserved in all dimensions:

$$\begin{aligned}
\frac{dE}{dt} &= \frac{1}{2} \frac{d}{dt} \int \mathbf{u}^2 d\mathbf{x} = \int \mathbf{u} \cdot \frac{\partial \mathbf{u}}{\partial t} d\mathbf{x} \\
&= \int \mathbf{u} \cdot (-\mathbf{u} \cdot \nabla \mathbf{u} - \nabla P) d\mathbf{x} = - \int \mathbf{u} \cdot \nabla \left( \frac{\mathbf{u}^2}{2} + P \right) d\mathbf{x} \\
&= \int (\nabla \cdot \mathbf{u}) \left( \frac{\mathbf{u}^2}{2} + P \right) d\mathbf{x} = 0
\end{aligned} \tag{1.5}$$

since  $\nabla \cdot \mathbf{u} = 0$ . In accord with Noether's theorem, energy conservation is related to the time-translation symmetry of (1.1). Similarly, the total momentum  $\int \mathbf{u} d\mathbf{x}$  is conserved because (1.1) is invariant with respect to translation in space.

Helicity,  $H = \int \mathbf{u} \cdot (\nabla \times \mathbf{u}) d\mathbf{x}$  is also conserved by (1.1) [Yahalom 1994]. Unlike energy, helicity is not positive definite, and the importance of its role

in turbulence is not clear [Bowman *et al.* 2006].

The domain in which we choose to work, and in which some of the major works in the subject have been set, is a square periodic box of length  $L$ . This approximation is often justified *a posteriori* by demonstrating that the numerically predicted turbulence correlation length is small compared with the box size. While this is obviously not a completely realistic assumption, calculations in such a domain are simpler and significant insight can nonetheless be gained into turbulence. Working in a periodic domain facilitates the use of Fourier transforms, which can be implemented by efficient (so-called *fast*) algorithms. The amplitude distribution of modes in Fourier space will be shown to be important in Section 2. For the time being, what is necessary is the form of the Navier–Stokes equation in Fourier space:

$$\frac{\partial \hat{\mathbf{u}}_{\mathbf{k}}}{\partial t} + \mathbf{k} (\hat{\mathbf{u}} * \hat{\mathbf{u}})_{\mathbf{k}} = -\mathbf{k} \hat{P}_{\mathbf{k}} - \nu k^2 \hat{\mathbf{u}}_{\mathbf{k}}. \quad (1.6)$$

Here  $\hat{\mathbf{u}}$  is the Fourier transform of  $\mathbf{u}$  and  $\hat{\mathbf{u}} * \hat{\mathbf{u}}$  is the wavenumber convolution of  $\hat{\mathbf{u}}$  with itself. We can solve for  $\hat{P}_{\mathbf{k}}$  by inverting a Laplacian:

$$\nabla^2 P = \nabla \cdot [\mathbf{F} - (\mathbf{u} \cdot \nabla) \mathbf{u}]. \quad (1.7)$$

Numerically, the complications of calculating the convolution in (1.6) are immense. It is advantageous to calculate this term in  $x$  space; this is known as the *pseudo-spectral* method [Gottlieb & Orszag 1977]. With the use of fast Fourier transforms, pseudo-spectral methods provide significant savings in computational cost.

In addition to computational ease, formulating the problem in Fourier space

makes it easy to confine the energy injection to certain scales. Typically, we are interested in a system where we have a known energy injection only on large scales. If we choose a white-noise force that is  $\delta$  correlated in time, we can control the average rate of energy injection, which we label  $\epsilon$ . The average rate of energy injection due to forcing is equal to

$$\epsilon = \frac{1}{2} \sum_{\mathbf{k}} \left\langle \frac{\partial |\mathbf{u}_{\mathbf{k}}|^2}{\partial t} \right\rangle = \text{Re} \sum_{\mathbf{k}} \left\langle \mathbf{u}_{\mathbf{k}}^* \frac{\partial \mathbf{u}_{\mathbf{k}}}{\partial t} \right\rangle = \text{Re} \sum_{\mathbf{k}} \langle \mathbf{u}_{\mathbf{k}}^* \mathbf{F}_{\mathbf{k}} \rangle = \frac{1}{2} \sum_{\mathbf{k}} |\mathbf{F}_{\mathbf{k}}|^2 \quad (1.8)$$

via Gaussian integration by parts, where  $*$  denotes complex conjugation. We refer interested readers to Novikov [1964] or Frisch [1995].

### 1.A.1 Reynolds number and scale independence

Osborn Reynolds introduced a parameter in 1883 based on the observations of flow through a pipe. The *Reynolds number* is  $R \doteq UL/\nu$ , where  $U$  is a typical velocity amplitude and  $L$  a characteristic length. When  $R$  is small, the fluid tends to move along clear, separated stream lines. Such flow is called *laminar*. When  $R$  is increased above a certain value, typically on the order of hundreds, the laminar flow is abruptly replaced first by boundary-layer phenomenon and, as  $R$  increases further, by fully turbulent flow. The Navier–Stokes equation is invariant under rescaling of time, space, velocity, and viscosity so long as  $R$  is held constant. That is, if we choose  $\lambda$  and  $\gamma$  to be non-zero real numbers and apply the mapping

$$(t, \mathbf{r}, \mathbf{u}, \nu) \rightarrow \left( \gamma t, \lambda \mathbf{r}, \frac{\lambda}{\gamma} \mathbf{u}, \frac{\lambda^2}{\gamma} \nu \right), \quad (1.9)$$

then (1.1) is mapped to

$$\frac{\partial \frac{\lambda}{\gamma} \mathbf{u}}{\partial \gamma t} + \frac{\lambda \mathbf{u}}{\gamma} \cdot \frac{\nabla \lambda \mathbf{u}}{\lambda \gamma} = - \frac{\nabla \lambda^2 P}{\lambda \gamma^2} + \frac{\lambda^2 \nu \nabla^2 \lambda \mathbf{u}}{\gamma \lambda^2 \gamma}, \quad (1.10)$$

which is just (1.1) multiplied by  $\lambda/\gamma^2$ . Note that the Reynolds number  $R = UL/\nu$  under this transformation is constant. This is a very interesting feature of the Navier–Stokes equation: scale-independence. The same equation can be used to model everything from microscopic flow to galactic dynamics. We are also cheered by the hope that arguments that we present may be applied at a variety of scales. Unfortunately, it is extraordinarily computationally difficult to simulate high-Reynolds number turbulence. In a three-dimensional system, the number of modes needed to capture the dynamics of the flow grows like  $R^{9/4}$ . Since there are physical systems (like the Earth’s atmosphere) with  $R \approx 10^{15}$ , researchers have been forced to apply various *ad hoc* methods to render the simulation tractable, typically by increasing the effect of viscosity in one way or another.

### 1.A.2 Turbulence in lower dimensions

While three-dimensional turbulence is of more interest and importance than turbulence in lower dimensions, two-dimensional turbulence is still highly non-trivial. Two-dimensional turbulence can be approximately realised in highly stratified fluids, e.g. atmospheric layers, or when the fluid is confined to a surface, e.g. the surface of a soap bubble. Like three-dimensional turbulence, turbulence in two dimensions conserves energy. However, the helicity is trivially conserved in two dimensions:  $H = \int \mathbf{u} \cdot \boldsymbol{\omega} d\mathbf{x} = 0$  because the *vorticity*  $\boldsymbol{\omega} \doteq \nabla \times \mathbf{u}$  is perpendicular to the plane of fluid motion. The vorticity plays

a more important role. If we take the curl of (1.1), we get

$$\frac{\partial \boldsymbol{\omega}}{\partial t} + \mathbf{u} \cdot \nabla \boldsymbol{\omega} = \boldsymbol{\omega} \cdot \nabla \mathbf{u} + \nu \nabla^2 \boldsymbol{\omega} + \nabla \times \mathbf{F}. \quad (1.11)$$

In two dimensions  $\boldsymbol{\omega} \cdot \nabla \mathbf{u} = \mathbf{0}$  since the gradient of the velocity must lie in the plane of the velocity, and  $\boldsymbol{\omega}$  is perpendicular to that plane. Thus, in two dimensions, we may write

$$\frac{\partial \boldsymbol{\omega}}{\partial t} + \mathbf{u} \cdot \nabla \boldsymbol{\omega} = \nu \nabla^2 \boldsymbol{\omega} + \nabla \times \mathbf{F}. \quad (1.12)$$

If  $\mathbf{F} = \mathbf{0}$  and  $\nu = 0$ , then the *enstrophy*  $Z = \frac{1}{2} \int \omega^2 d\mathbf{x}$  is conserved with zero or periodic boundary conditions:

$$\begin{aligned} \frac{dZ}{dt} &= \int \boldsymbol{\omega} \cdot \frac{\partial \boldsymbol{\omega}}{\partial t} d\mathbf{x} = \int \boldsymbol{\omega} \cdot (-\mathbf{u} \cdot \nabla) \boldsymbol{\omega} d\mathbf{x} \\ &= \int (\nabla \cdot \mathbf{u}) \frac{\omega^2}{2} d\mathbf{x} = 0 \end{aligned} \quad (1.13)$$

since  $\nabla \cdot \mathbf{u} = 0$ . Unlike helicity, enstrophy is positive-semidefinite and plays an important role in two-dimensional turbulence. In fact, the spatial integral of any continuously differentiable function of the vorticity is conserved by the two-dimensional Navier–Stokes equation. Such conserved quantities are known as *Casimir invariants* (e.g. see [Morrison 1998]). However, only energy and enstrophy are conserved by systems with a finite number of Fourier modes. The additional invariants are not respected by numerical simulations that necessarily truncate the spectrum.

Our hopes buoyed by reformulating the problem in two dimensions, we are tempted to move to one-dimensional turbulence. Certainly, one-dimensional

turbulence is much more amenable to numerical simulation and more susceptible to attack by analytic means. This is, in fact, more true than we had hoped; incompressible one-dimensional turbulence is too simple. In this case mass conservation and incompressibility give  $\partial u(x, t)/\partial x = 0$ , which implies that the velocity is uniform, providing little insight into higher-dimensional turbulence. Thus, if we wish to study some type of one-dimensional turbulence, we cannot consider the incompressible Navier–Stokes equation directly but must instead consider some analogous system.

## 1.B Shell models of turbulence

While one-dimensional Navier–Stokes turbulence turns out not to be turbulent, there are a plethora of other systems that we can consider. In addition to being useful caricatures of Navier–Stokes turbulence, these models are interesting in their own right, much as the case of two-dimensional Navier–Stokes turbulence. Also, some models can be tailored to mimic turbulence in either two or three dimensions. Generally, these models have just one active (complex) mode, say  $u_n$ , which represents either an average value or a total value for all Fourier amplitudes in a wavenumber shell  $n$  of minor radius  $k_n$ . In all the models that are discussed in this section,  $k_n = k_0 \lambda^n$ , which allows one to cover a very wide range in Fourier space with very few modes. These systems are still very stiff; typical time scales of the slowest and fastest modes in simulations found in the literature are separated by a factor  $10^6$  or  $10^9$  [L’vov *et al.* 1998], [Bowman *et al.* 2006]. The shell models in this section are governed by an

equation of the form

$$\frac{\partial u_n}{\partial t} + \nu k_n^2 u_n = ik_n \sum_{\ell, m} A_{\ell, m} u_\ell^* u_m^* + F_n, \quad (1.14)$$

where  $\nu$  is the coefficient of linear viscosity,  $i^2 = -1$ ,  $A_{\ell, m}$  is a (possibly complex) coupling coefficient, and  $F_n$  is the external force on mode  $n$ . We will consider three shell models in this thesis; the DN model, the GOY model, and the Sabra model.

### 1.B.1 DN model

While intermodal interactions in Navier–Stokes turbulence are non-local in Fourier space, the cumulative energy transfer is often seen as a cascade [Biferale 2003], where energy moves between adjacent shells. From this point of view, the most important interactions are between modes in adjacent shells. It is then natural to create a shell model that includes only nearest-neighbour interactions. In fact, if one requires that the nonlinearity be quadratic in the complex conjugate of the velocity (as in (1.14)) and that energy be conserved in the absence of forcing and dissipation, one arrives at the model proposed by Desnyansky and Novikov [Desnyansky & Novikov 1974]. We will refer to this model as the DN model.

Let  $u_n$ ,  $n = 0, \dots, N - 1$  be the complex-valued Fourier modes. For convenience, we set  $u_n = 0$  for all modes with  $n < 0$  or  $n \geq N$ . The equation governing the shell velocities is

$$\begin{aligned} \frac{\partial u_n}{\partial t} = & (A_n u_{n+1}^2 + B_n u_n u_{n+1} + C_n u_{n-1} u_{n+1} + D_n u_{n-1} u_n + E_n u_{n-1}^2)^* \\ & - \nu k_n^2 u_n + F_n, \end{aligned} \quad (1.15)$$

where  $*$  represents complex conjugation, and the parameters  $A_n, B_n, C_n, D_n$ , and  $E_n$  are *coupling coefficients*. Such a system has energy  $E \doteq \frac{1}{2} \sum_n |u_n|^2$ . The rate of change of energy due to the nonlinear terms is

$$\begin{aligned}
\frac{dE}{dt} &= \operatorname{Re} \sum_{n=0}^{N-1} u_n \frac{\partial u_n^*}{\partial t} \\
&= \operatorname{Re} \sum_{n=0}^{N-1} (A_n u_n u_{n+1}^2 + B_n u_n^2 u_{n+1} + C_n u_{n-1} u_n u_{n+1} + D_n u_{n-1} u_n^2 \\
&\quad + E_n u_{n-1}^2 u_n) \\
&= \operatorname{Re} \left\{ C_0 \cancel{u_{-1}}^0 u_0 u_1 + D_0 \cancel{u_{-1}}^0 u_0^2 + E_0 \cancel{u_{-1}}^0 u_0 \right. \\
&\quad + \sum_{n=1}^{N-2} [(A_n + D_{n+1}) u_n u_{n+1}^2 + (B_n + E_{n+1}) u_n^2 u_{n+1} + C_n u_{n-1} u_n u_{n+1}] \\
&\quad \left. + A_{N-1} u_{N-1} \cancel{u_N}^0 + B_{N-1} u_{N-1}^2 \cancel{u_N}^0 + C_{N-1} u_{N-2} u_{N-1} \cancel{u_N}^0 \right\}.
\end{aligned} \tag{1.16}$$

In order for the above sum to telescope to zero for all  $u_n$ , it is necessary for  $n = 1, \dots, N - 2$  that  $C_n = 0$ ,  $A_n = -D_{n+1}$ , and  $B_n = -E_{n+1}$ . That is,

$$\frac{\partial u_n}{\partial t} + \nu k_n^2 u_n = (A_n u_{n+1}^2 + B_n u_{n+1} u_n - A_{n-1} u_n u_{n-1} - B_{n-1} u_{n-1}^2)^* + F_n. \tag{1.17}$$

To mimic the appearance of the Navier–Stokes equation, which has a derivative as part of its nonlinearity, we extract an overall factor of  $ik_n$  from the

coefficients  $A_n$  and  $B_n$ ; this allows us to write the DN model in the form

$$\frac{\partial u_n}{\partial t} + \nu k_n^2 u_n = ik_n (a_n u_{n-1}^2 - \lambda a_{n+1} u_n u_{n+1} + b_n u_{n-1} u_n - \lambda b_{n+1} u_{n+1}^2)^* + F_n. \quad (1.18)$$

Let us specialise to the case where  $a_n = a \in \mathbb{R}$  and  $b_n = b \in \mathbb{R}$  for  $n = 0, \dots, N-1$ . The *energy spectrum* (or *energy density*)  $E(k)$  is defined according to

$$E(k_n) \doteq \frac{1}{2} \frac{|u_n|^2}{k_{n+1} - k_n}.$$

For uniform  $u_n$ ,  $E(k) \sim k^{-1}$  since the wavenumbers  $k_n$  are spaced geometrically.

The nonlinearity of the DN model has a fixed point at  $u_n \sim k_n^{-1/3}$ :

$$\frac{\partial u_n}{\partial t} = ik_n \left( a \lambda^{\frac{2}{3}} u_n^2 - \lambda a \lambda^{-\frac{1}{3}} u_n^2 + b \lambda^{\frac{1}{3}} u_n^2 - \lambda b \lambda^{-\frac{2}{3}} u_n^2 \right)^* = 0 \quad (1.19)$$

since  $k_{n+1}/k_n = \lambda$ . Bell & Nelkin [1977] concluded for the case where  $a$  and  $b$  are of opposite signs that this fixed point is linearly stable. It is associated with an energy spectrum  $E(k) \sim k^{-5/3}$  that is reminiscent of the Kolmogorov spectrum for three-dimensional turbulence [Kolmogorov 1941a], as detailed in Chapter 2. Also, the DN model can be made to conserve helicity (or enstrophy) only under the trivial conditions  $a = b = 0$  or  $\lambda = 1$ . For this and similar reasons, it is generally thought that the DN model is too simple to model three-dimensional turbulence effectively. It has been largely superseded by the GOY model.

## 1.B.2 GOY model

The GOY model is named after Gledzer, Ohkitana, and Yamada. A real version was proposed by Gledzer [1973], and the complex version was proposed by Yamada & Ohkitani [1987]. The GOY model was designed as a model of three-dimensional turbulence that, while it acts as an analog of the Navier–Stokes equation, is not intended as a result that one can derive from the Navier–Stokes equation, and Yamada and Ohkitani state that “no special attention will be paid to the justification of our model equation.” Unlike the DN model, the GOY model is not a necessary result of a set of requirements, and there is at least one competing model. GOY turbulence resembles three- (or two-) dimensional Navier–Stokes turbulence in at least four respects [Kadanoff *et al.* 1995]:

1. In the absence of dissipation and forcing, energy and helicity (or enstrophy) are conserved.
2. The nonlinear source term preserves phase volume (cf. Chapter 3).
3. The system can reach a statistically steady state in which it behaves chaotically.
4. The multi-fractal behaviour bears striking resemblance to experimental observations of three-dimensional turbulence. In addition to these points, the main benefit of studying the GOY model is that results (such as Kolmogorov’s four-fifth’s law [Frisch 1995]) for the Navier–Stokes equation should apply equally well to shell models, which are more amenable to further analysis.

Like the DN model, the GOY model conserves energy, and has a source term that is quadratic in the complex conjugate of the velocity field. While the DN model has nearest-neighbour interactions, the GOY model has next-nearest neighbour interactions. The governing equation of the GOY model is

$$\frac{\partial u_n}{\partial t} = ik_n \left( \alpha u_{n+1} u_{n+2} + \frac{\beta}{\lambda} u_{n-1} u_{n+1} + \frac{\gamma}{\lambda^2} u_{n-1} u_{n-2} \right)^* - \nu k_n^2 u_n + F_n, \quad (1.20)$$

where  $\alpha$ ,  $\beta$ , and  $\gamma$  are real coupling coefficients. As in the DN model, the wavenumbers  $k_n = k_0 \lambda^n$  scale geometrically, and the complex velocities  $u_n$  are said to be “associated with” [Yamada & Ohkitani 1987] the wavenumber  $k_n$ . Like the DN model, the GOY model has a fixed point at  $u_n \sim k_n^{-1/3}$ , but this fixed point is not stable [Biferale *et al.* 1995]. For this reason, it is thought that the GOY model may imitate the intermittent behaviour of full Navier–Stokes turbulence better than the DN model [Benzi *et al.* 2004].

The GOY model exhibits different behaviours depending on the choice of the parameters  $\alpha$ ,  $\beta$ ,  $\gamma$ , and  $\lambda$ . Normally, one chooses such coefficients based on the physics governing the problem in question. Since the GOY model is a toy model of turbulence, we look to the Navier–Stokes equation to provide some insight. Firstly, we require that the energy be conserved. As in the DN model, a telescoping sum can be used to establish that  $\alpha + \beta + \gamma = 0 \Rightarrow dE/dt = 0$ . It is conventional to rescale time so that  $\alpha = 1$ , which leaves two free parameters, say  $\beta$  and  $\lambda$ . With different combinations of  $\beta$  and  $\lambda$ , different quantities are

conserved. The second conserved quantity is

$$\frac{1}{2} \sum_n k_n^p |u_n|^2, \quad (1.21)$$

where  $p \doteq -\log_\lambda(-\beta - 1)$ . Typically, we choose  $\lambda$ , the spacing between wavenumbers, to be 2. In this standard case, the choice  $\beta = -1/2$  gives the second conserved quantity the form of helicity in the three-dimensional Navier–Stokes equation:

$$H = \frac{1}{2} \sum_n (-1)^n k_n |u_n|^2. \quad (1.22)$$

If  $\beta = -5/4$ , then the GOY model instead conserves vorticity, as does the two-dimensional Navier–Stokes equation:

$$Z = \frac{1}{2} \sum_n k_n^2 |u_n|^2. \quad (1.23)$$

Clearly, the Fourier-space structure of the GOY model and Navier–Stokes turbulence are very different. This may lead to some anomalies in the energy spectrum for the GOY model that are inconsistent with the behaviour of the Navier–Stokes equation. In particular, modes are uncorrelated in Navier–Stokes turbulence:

$$\langle \mathbf{u}_k \mathbf{u}_p^* \rangle = |\mathbf{u}_k|^2 \delta_{k,p}. \quad (1.24)$$

This is not the case in the GOY model, which has a period-three oscillation in  $u_n$  [Biferale *et al.* 1995], as evident from the fact that

$$u_n = k_n^{-\frac{1}{3}} \begin{cases} A_0 & \text{for } n = 0 \pmod{3}, \\ A_1 & \text{for } n = 1 \pmod{3}, \\ A_2 & \text{for } n = 2 \pmod{3} \end{cases} \quad (1.25)$$

is a fixed point of the nonlinearity for arbitrary complex amplitudes  $A_0$ ,  $A_1$ , and  $A_2$ . This means that some modes are correlated:

$$\langle u_n u_{n+3p}^* \rangle \neq 0 \quad \text{for } p \in \mathbb{Z}. \quad (1.26)$$

However, both  $\langle u_n u_{n+3p+1}^* \rangle$  and  $\langle u_n u_{n+3p+2}^* \rangle$  lack correlation, in agreement with Navier–Stokes behaviour. These period-three oscillations insert noise into the spectrum  $E(k)$ . Since one of the main reasons to study shell models is to eliminate uncertainty in the power-law relation between  $E(k)$  and  $k$ , this is a drawback to the GOY model. Kadanoff, Lohse, Wang, and Benzi [Kadanoff *et al.* 1995] proposed that the second-order scaling exponent may be better calculated using the *flux*, which they defined as

$$\Sigma_n = \left\langle \left| \text{Im} \left( u_n u_{n+1} u_{n+2} + \frac{1+\beta}{\lambda} u_{n-1} u_n u_{n+1} \right) \right|^{2/3} \right\rangle. \quad (1.27)$$

As may be seen in the logarithmic spectral slopes plotted in Fig. 1.1, this does indeed produce a smoother spectrum. Since scaling exponents are calculated when the flow has reached a statistical steady state, the flux is useful in isolating statistical error from the period-three oscillation.

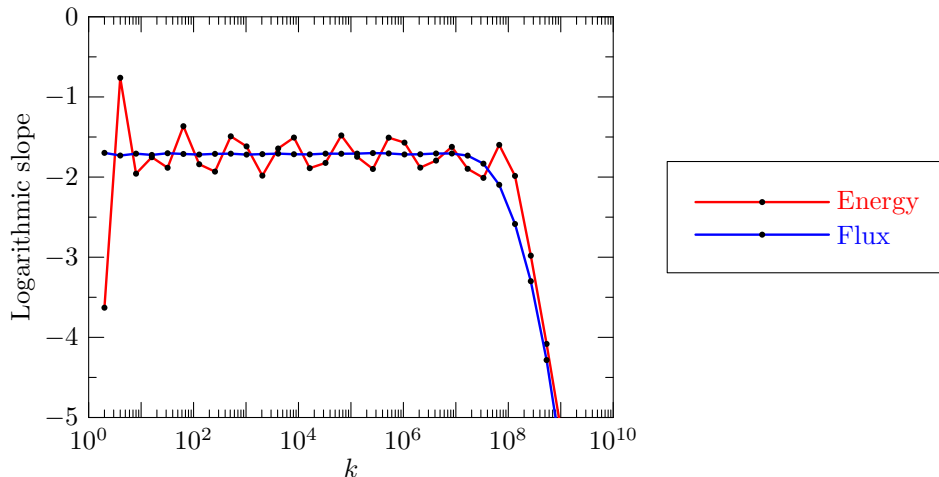


Figure 1.1: Comparison of the logarithmic slopes of the energy and flux spectra for the GOY model.

### 1.B.3 Sabra model

L'vov *et al.* [1998] introduced the Sabra shell model in an attempt to solve the problem of anomalous correlation in the GOY model. The Sabra model is based on the GOY model, but does not take the complex conjugate of all the modes in the nonlinear source term. The governing equation for the Sabra model is

$$\frac{\partial u_n}{\partial t} = ik_n \left( \alpha u_{n+2} u_{n+1}^* + \frac{\beta}{\lambda} u_{n+1} u_{n-1}^* - \frac{\gamma}{\lambda^2} u_{n-1} u_{n-2} \right) - \nu k_n^2 u_n + F_n. \quad (1.28)$$

Most of the properties of the GOY and Sabra models are identical, except that  $\langle u_n u_{n+3p}^* \rangle = 0$  for the Sabra model. Because of this, the period-three oscillations in  $E(k)$  are absent for the Sabra model, which eliminates the need to base scaling exponents on the flux introduced by Kadanoff *et al.* The Sabra model has a fixed point at  $u_n = u_0 k_n^{-1/3}$ . However,  $u_0$  must be either entirely

real or entirely imaginary to be a fixed point of the Sabra model, whereas the GOY model places no restriction on the phase of the fixed point. Unlike the Navier–Stokes equation, the nonlinearity in the Sabra model depends on both the velocity and the complex conjugate of the velocity itself, whereas the Navier–Stokes equation, the GOY model, and the DN model are quadratic only in the complex conjugate of the velocity.

# Chapter 2

## Kolmogorov Theory

*In which we reproduce some classic results and extend them to shell models.*

The viscous term in the Navier–Stokes equation is predominantly active at the small scales, where it acts to remove energy, while energy injection (via forcing) is typically restricted to large scales. In statistically steady three-dimensional turbulence, the energy is transferred by the nonlinear (advective) term from the large scales to the small scales. The region of Fourier space in which this energy transfer takes place, in the absence of forcing and dissipation, is called the *inertial range*.

Given the energy injection rate  $\epsilon$ , the scale  $\ell$  at which it is injected and the coefficient of viscosity,  $\nu$ , we would like to predict the scaling of the energy spectrum

$$E(k) = \frac{1}{2} \frac{1}{(2\pi)^3} \int_0^{2\pi} \int_0^\pi |\mathbf{u}_{\mathbf{k}}|^2 k^2 \sin \theta d\theta d\phi \quad (2.1)$$

with wavenumber  $k$  in the inertial range. Note that  $E(k)$  is normalised so

that the one-dimensional integral  $\int E(k) dk$  evaluates to the total energy  $E$ . As a first step, it is useful to look at this problem with dimensional analysis. Kolmogorov argued that only the typical velocity magnitude  $u$ , the energy injection rate  $\epsilon$ , and the Fourier wavenumber  $k$  are relevant. Dimensional consistency gives  $\epsilon \sim u^3 k$ , so  $u \sim (\epsilon/k)^{1/3}$  and  $u^2 \sim (\epsilon/k)^{2/3}$ . But  $u^2 = 2 \int E(k) dk$  has the same dimensions as  $kE(k)$ , so

$$E(k) = Ck^{-1} \left( \frac{\epsilon}{k} \right)^{\frac{2}{3}} = C\epsilon^{\frac{2}{3}} k^{-\frac{5}{3}} \quad (2.2)$$

for some dimensionless quantity  $C$ . This result was established by Kolmogorov [1941a], who conjectured that  $C$  is a universal constant for all fully developed turbulent flows. While this is the simplest argument for Kolmogorov's five-thirds law, the result can be attained in a more systematic fashion from a few hypotheses.

Kolmogorov's 1941 papers analysed the various statistical moments of Navier–Stokes turbulence. He used three universality assumptions, which we label K1, K2, and K3 [Kolmogorov 1941a], [Kolmogorov 1941b], [Frisch 1995].

K1: The statistical moments  $\langle \mathbf{f}(\mathbf{u}) \rangle$ , where  $\langle \rangle$  denotes an ensemble average, are determined by the energy injection rate  $\epsilon$  and viscosity  $\nu$ .

K2: If  $\mathbf{r}$  and  $\boldsymbol{\ell}$  are smaller than the integral scale, the velocity increments

$$\delta \mathbf{u}(\mathbf{r}, \boldsymbol{\ell}) \doteq \mathbf{u}(\mathbf{r} + \boldsymbol{\ell}) - \mathbf{u}(\mathbf{r}) \quad (2.3)$$

scale like

$$\delta \mathbf{u}(\mathbf{r}, \lambda \boldsymbol{\ell}) = \lambda^h \delta \mathbf{u}(\mathbf{r}, \boldsymbol{\ell}) \quad \forall \lambda > 0. \quad (2.4)$$

K3: On scales much larger than those where friction removes energy from the system, the statistical moments are determined by the energy injection rate  $\epsilon$  alone.

Kolmogorov took the case of infinite Reynolds number limit by letting time  $t \rightarrow \infty$ , then  $\nu \rightarrow 0$ , and finally  $\ell \rightarrow 0$ , thus dealing with fully developed turbulence, in the limit of zero viscosity, and at the small scales. He considered the moments

$$S_p(\ell) \doteq \langle |\delta \mathbf{u}_{\parallel}(\ell)|^p \rangle \quad (2.5)$$

of the parallel velocity increment

$$\delta \mathbf{u}_{\parallel}(\mathbf{r}, \boldsymbol{\ell}) \doteq (\mathbf{u}(\mathbf{r} + \boldsymbol{\ell}) - \mathbf{u}(\mathbf{r})) \cdot \frac{\boldsymbol{\ell}}{\ell}. \quad (2.6)$$

Note that for homogeneous and isotropic fluids the moments  $S_p$  do not depend on  $\mathbf{r}$  or the direction of  $\boldsymbol{\ell}$ . For the special case  $p = 3$ , Kolmogorov derived an exact relation, known as the *four-fifths law*:

$$S_3(\ell) = -\frac{4}{5}\epsilon\ell, \quad (2.7)$$

for  $\ell$  in the inertial range. He conjectured that a similar dimensionally consistent result holds for all  $p$ :

$$S_p(\ell) = C_p \epsilon^{\frac{p}{3}} \ell^{\frac{p}{3}}, \quad (2.8)$$

where  $C_p$  is a constant. With regards to the perpendicular velocity increment,

$$\delta\mathbf{u}_\perp(\mathbf{r}, \boldsymbol{\ell}) \doteq (\mathbf{u}(\mathbf{r} + \boldsymbol{\ell}) - \mathbf{u}(\mathbf{r})) \cdot \hat{\mathbf{n}}, \quad (2.9)$$

where  $\hat{\mathbf{n}}$  is a unit vector perpendicular to  $\boldsymbol{\ell}$  (the direction does not matter otherwise due to isotropy), Kolmogorov [1941a] showed that

$$\langle |\delta\mathbf{u}_\perp(\mathbf{r}, \boldsymbol{\ell})|^2 \rangle = 2S_2(\ell), \quad (2.10)$$

which, given (2.8) together with the Wiener-Khinchin formula

$$E(k) = \frac{1}{\pi} \int_0^\infty k\ell \langle \mathbf{u}(\mathbf{r}) \cdot \mathbf{u}(\mathbf{r} + \boldsymbol{\ell}) \rangle \sin k\ell \, d\ell, \quad (2.11)$$

implies that

$$E(k) \sim k^{-\frac{5}{3}}, \quad (2.12)$$

which has been shown experimentally to be at least approximately true. Corrections to this law, however, are a subject of much ongoing research [Nelkin 2001], [Boffetta & Romano 2002].

Landau objected to Kolmogorov's arguments, saying that the constant  $C_p$  in (2.8) need not be universal. Kolmogorov answered Landau's objections in his third paper of 1941. Since then, Kolmogorov's arguments have been reformulated based on more convincing assumptions. We shall provide below a brief summary of the derivation of (2.7) given by Frisch [1995].

Starting with a description of the inertial range, Frisch defines the energy transfer due to the nonlinearity, i.e. due to advection and pressure, which he

denotes

$$\epsilon(\ell) \doteq -\frac{1}{2}\partial_t \langle \mathbf{u}(\mathbf{r}) \cdot \mathbf{u}(\mathbf{r} + \boldsymbol{\ell}) \rangle |_{\text{NL}}. \quad (2.13)$$

Since the nonlinear terms conserve energy, we see that  $\epsilon(0) = 0$ . One then makes use of the Kármán–Howarth–Monin relation [de Kármán & Howarth 1937], [Monin & Yaglom 1965]:

$$\begin{aligned} \epsilon(\ell) &= -\frac{1}{4}\nabla_{\boldsymbol{\ell}} \cdot \langle |\delta\mathbf{u}(\boldsymbol{\ell})|^2 \delta\mathbf{u}(\boldsymbol{\ell}) \rangle \\ &= -\partial_t \frac{1}{2} \langle \mathbf{u}(\mathbf{r}) \cdot \mathbf{u}(\mathbf{r} + \boldsymbol{\ell}) \rangle + \left\langle \mathbf{u}(\mathbf{r}) \cdot \frac{\mathbf{f}(\mathbf{r} + \boldsymbol{\ell}) + \mathbf{f}(\mathbf{r})}{2} \right\rangle \\ &\quad + \nu \nabla_{\boldsymbol{\ell}}^2 \langle \mathbf{u}(\mathbf{r}) \cdot \mathbf{u}(\mathbf{r} + \boldsymbol{\ell}) \rangle. \end{aligned} \quad (2.14)$$

By taking  $\ell \rightarrow 0$  (but holding  $\nu$  constant) and assuming that the velocity field is smooth, one concludes from the fact that  $\epsilon(0) = 0$  that the term  $\nabla_{\boldsymbol{\ell}} \cdot \langle |\delta\mathbf{u}(\boldsymbol{\ell})|^2 \delta\mathbf{u}(\boldsymbol{\ell}) \rangle$  goes to zero. That is, at very small scales, we have

$$\frac{1}{2}\partial_t \langle \mathbf{u}^2 \rangle = \langle \mathbf{f}(\mathbf{r}) \cdot \mathbf{u}(\mathbf{r}) \rangle + \nu \langle \mathbf{u}(\mathbf{r}) \cdot \nabla^2 \mathbf{u}(\mathbf{r}) \rangle. \quad (2.15)$$

We now calculate the energy flux. Define  $\Pi_K$  to be the flux of from all modes with  $|\mathbf{k}| \leq K$  to all modes with  $|\mathbf{k}| > K$ . Then we can relate  $\Pi_k$  to  $\epsilon(\ell)$  by

$$\begin{aligned} \Pi_K &= -\frac{1}{8\pi^2} \int \frac{\sin(K\ell)}{\ell} \nabla_{\boldsymbol{\ell}} \cdot \left( \frac{\boldsymbol{\ell}}{\ell^2} \nabla_{\boldsymbol{\ell}} \cdot \langle |\delta\mathbf{u}(\boldsymbol{\ell})|^2 \delta\mathbf{u}(\boldsymbol{\ell}) \rangle \right) d\boldsymbol{\ell} \\ &= \frac{1}{2\pi^2} \int \frac{\sin(K\ell)}{\ell} \nabla_{\boldsymbol{\ell}} \cdot \left( \epsilon(\ell) \frac{\boldsymbol{\ell}}{\ell^2} \right) d\boldsymbol{\ell}. \end{aligned} \quad (2.16)$$

Finally, for isotropic homogeneous turbulence, the energy flux can be written

as

$$\Pi_K = -\frac{1}{6\pi} \int_0^\infty \frac{\sin(K\ell)}{\ell} (1 + \ell\partial_\ell)(3 + \ell\partial_\ell)(5 + \ell\partial_\ell) \frac{S_3(\ell)}{\ell} d\ell, \quad (2.17)$$

which implies that

$$\epsilon(\ell) = -\frac{1}{12} (3 + \ell\partial_\ell)(5 + \ell\partial_\ell) \frac{S_3(\ell)}{\ell}. \quad (2.18)$$

While this formulation of the four-fifths law has fewer, more plausible assumptions than those originally made by Kolmogorov, it is not assumption-free. The assumptions that we must make are:

- H1: The driving force  $\mathbf{f}(\mathbf{r}, t)$  acts at the large scales. That is, we assume it to be equal to its low-pass filter if we pass all frequencies below the frequency corresponding to the integral scale.
- H2: We assume that all solutions to the Navier-Stokes equation eventually reaches a statistically steady state with a finite mean energy.
- H3: In the limit of  $\nu \rightarrow \infty$ , we assume that the energy dissipation rate per unit mass attains a non-zero limit. That is,

$$\epsilon(\ell) \rightarrow \epsilon \doteq \lim_{K \rightarrow \infty} \Pi_K > 0 \text{ as } \nu \rightarrow 0. \quad (2.19)$$

Hypothesis H3 implies that the energy transfer rate must also be constant as  $\nu \rightarrow 0$ . In fact, the energy transfer must be uniform in the inertial range. Combining this fact with (2.17) yields

$$\epsilon = -\frac{1}{6\pi} \lim_{K \rightarrow \infty} \int_0^\infty \frac{\sin(K\ell)}{\ell} (1 + \ell\partial_\ell)(3 + \ell\partial_\ell)(5 + \ell\partial_\ell) \frac{S_3(\ell)}{\ell} d\ell \quad (2.20)$$

For large  $K$ , the integrand only contributes for small  $\ell$ . If we take the limit as  $\ell \rightarrow 0$  and assume some smoothness of the moment  $S_3$ , one obtains the desired result [Frisch 1995]:

$$S_3(\ell) = -\frac{4}{5}\epsilon\ell. \tag{2.21}$$

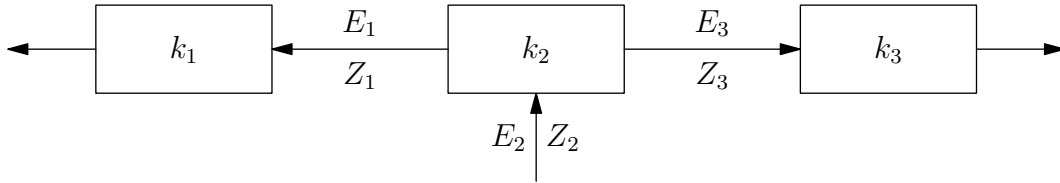
The four-fifths law explicitly establishes  $C_3 = -4/5$ , so there is no doubt as to its universality. For all other moments, we do not have such a result. In particular,  $C_p$  may depend on the integral scale and  $\ell$ , which we cannot rule out on dimensional grounds alone.

## 2.A Application to two-dimensional turbulence

The study of two-dimensional turbulence can provide insights into structure-function scaling exponents at Reynolds numbers that we would be unable to attain for three-dimensional turbulence. Unfortunately, the comparison is not exact, as forced-dissipative two-dimensional turbulence has a different behaviour than its three-dimensional cousin.

The two-dimensional energy cascade is complicated by enstrophy conservation. Unlike helicity, enstrophy is positive-semidefinite, and thus plays a much more important role in two-dimensional turbulence than helicity does in three dimensions. Because of this, we must not only consider the energy injection rate  $\epsilon$ , but also the enstrophy injection rate  $\eta$ . A white-noise Gaussian force has a Novikov theorem [Novikov 1964] for enstrophy injection as well, which allows one to control the enstrophy injection rate in the same fashion as one controls the energy injection rate.

The first results on the two-dimensional turbulent cascade were made by Kraichnan, Leith, and Batchelor, who considered truncated two-dimensional Navier–Stokes systems [[Kraichnan 1967], [Batchelor 1969], [Kraichnan 1971], [Kraichnan 1975]]. In particular, they considered interactions that are local in Fourier space, so that modes would only interact with other modes if they were in adjacent narrow bins in wavenumber-space. The picture of the energy and enstrophy cascades, first proposed by Fjørtoft [1953], is shown in Fig. 2.1. Energy and enstrophy are injected into the middle bin. Due to the inter-



Energy and Enstrophy Injection

Figure 2.1: Fjørtoft diagram.

actions between bins (which are assumed to be between neighbouring bins) energy and enstrophy move from the injection point to neighbouring bins. An amount of energy  $E_1$  moves from the middle bin to lower wavenumbers. As energy moves, so does enstrophy, which we label  $Z_1$ . Since the movement is to lower wavenumbers, and vorticity varies as  $k^2$ , enstrophy conservation can only occur if some energy, which we label  $E_2$ , is transferred to higher wavenumbers. With enstrophy transfer comes energy transfer. If  $k_1$ ,  $k_2$ , and  $k_3$  are typical wavenumber for the boxes, then the equations describing the balance of energy

and enstrophy transfers are

$$E_2 = E_1 + E_3, \quad (2.22)$$

$$Z_2 = Z_1 + Z_3, \quad (2.23)$$

that is,

$$E_2 = E_1 + E_3, \quad (2.24)$$

$$k_2^2 E_2 = k_1^2 E_1 + k_3^2 E_3. \quad (2.25)$$

This implies that

$$E_1 = E_2 \frac{k_3^2 - k_2^2}{k_3^2 - k_1^2}. \quad (2.26)$$

If we choose  $k_1 = k$ ,  $k_2 = 2k$ , and  $k_3 = 4k$ , then we should expect

$$E_1 = \frac{4}{5} E_2, \quad (2.27)$$

$$E_3 = \frac{1}{5} E_2.$$

Thus, we expect to see a bi-directional cascade with energy moving primarily to lower wavenumbers and enstrophy moving to higher wavenumbers. In an unbounded domain, the modes around  $\mathbf{k} = \mathbf{0}$  act as an infinite reservoir that the energy cascade cannot saturate. In this case, one expects a  $k^{-5/3}$  inverse cascade (as illustrated in Fig. 2.2) and a  $k^{-3}$  direct cascade.

However, Tran & Shepherd [2002] and Tran & Bowman [2003] showed that, for fluids in a bounded domain, the cascade proposed by Kraichnan is not realisable. In particular, the absence of an infinite reservoir near  $\mathbf{k} = \mathbf{0}$  means

that the spectrum will eventually saturate this region. They considered an idealised dual cascade of the form

$$E(k) = \begin{cases} ak^{-\alpha} & \text{for } k \leq s, \\ bk^{-\beta} & \text{for } k > s, \end{cases} \quad (2.28)$$

where  $\alpha$ ,  $\beta$ ,  $a$ , and  $b$  are constants and  $s$  is the forcing wavenumber. The two cascades are intricately linked via the balance equation

$$\sum_{k < s} (s^2 - k^2) \nu k^2 E(k) = \sum_{k > s} (k^2 - s^2) \nu k^2 E(k). \quad (2.29)$$

Tran and Bowman used this balance equation to show, given plausible assumptions, that

$$\alpha + \beta \leq 8, \quad (2.30)$$

where the inequality approaches an equality at high Reynolds number as the wavenumber domain approaches  $[0, \infty)$ . In this picture, the large-scale spectrum behaves like  $E(k) \sim k^{-3}$ , which implies that the small-scale spectrum behaves like  $E(k) \sim k^{-5}$ . An example of this is illustrated in Fig. 2.3 [Tran & Bowman 2003].

While Kraichnan's prediction may still hold for unbounded two-dimensional turbulence, numerical simulations are subject to the limits of computer memory and speed, and unbounded domains will remain out of the reach of numerical experiment. It has been suggested that systems be damped on the large scales, with either an inverse viscous force  $\nu_\mu k^{2\mu}$  with  $\mu < 0$ , or a constant viscous force restricted to low wavenumbers. Such large-scale damping has

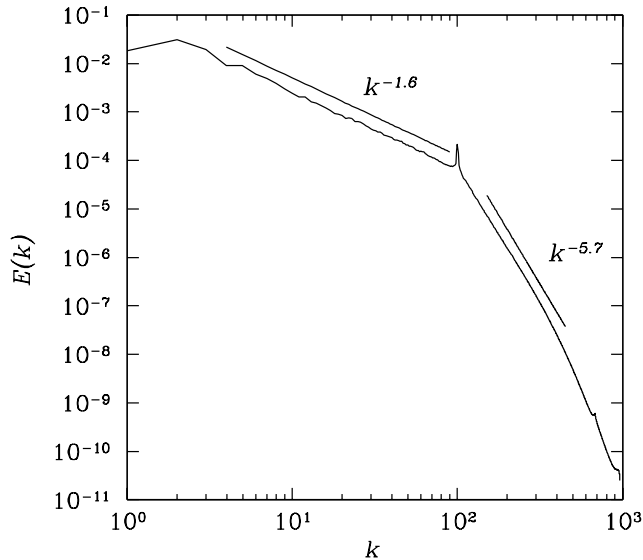


Figure 2.2: The 2D Navier–Stokes energy spectrum at intermediate times.

been suggested in the study of some planetary flows.

## 2.B Application to shell models

An energy spectrum with  $E(k) \sim k^{-5/3}$  is a fixed point of the DN, GOY, and Sabra shell models. While the cascade spectra shown for Navier–Stokes turbulence are not fixed points of the Navier–Stokes equation, they are fixed points of the energy spectrum  $E(k)$  in a statistical sense. Shell models, owing to their relative computational ease, are of course excellent testbeds for determining spectra. For example, the two-dimensional Navier–Stokes equation in a bounded domain appears asymptotically to approach a  $k^{-3}$  slope at the large scales, but this requires extraordinarily long run times. We would be able to approach such a spectrum more closely if we could recreate this behaviour with shell models. Despite this, certain shell models reproduce the intermittent corrections of three-dimensional turbulence surprisingly well

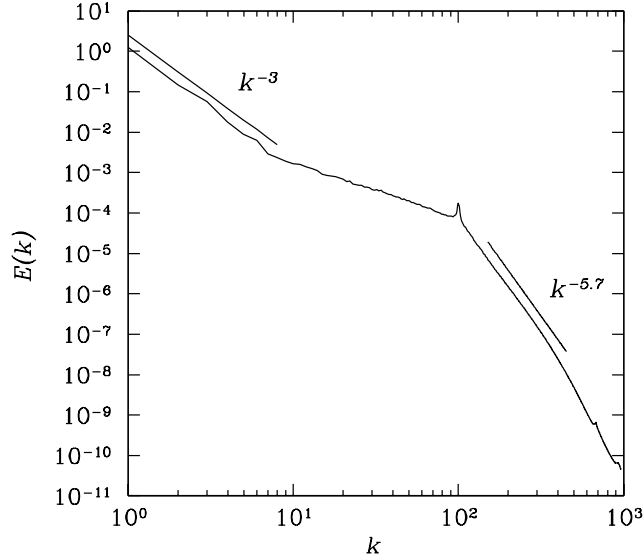


Figure 2.3: The 2D Navier–Stokes energy spectrum at late times.

[Bowman *et al.* 2006]. In particular, for  $\beta = -1/2$ , the three-dimensional GOY model is able to predict the scaling exponents  $\zeta_p$  for the structure functions  $S_p(k_n) = \langle |u_n|^p \rangle \sim k_n^{-\zeta_p}$  despite the dissimilarity of the underlying equations. A comparison of the predicted structure-function exponents with those measured experimentally by [Herweijer & van de Water 1995] is shown in Fig. 2.4.

Unfortunately, since a Kolmogorov  $k^{-5/3}$  energy spectrum is built into the shell models, they are not able to reproduce other spectra effectively. In particular, the two-dimensional version of the GOY model is not able to reproduce the dual cascade of two-dimensional forced-dissipative turbulence.

## 2.C Final comments on Kolmogorov’s results.

One very practical result of Kolmogorov’s work is his prediction of the dissipation scale  $k_d$ . This is the point where the viscous damping comes to dominate

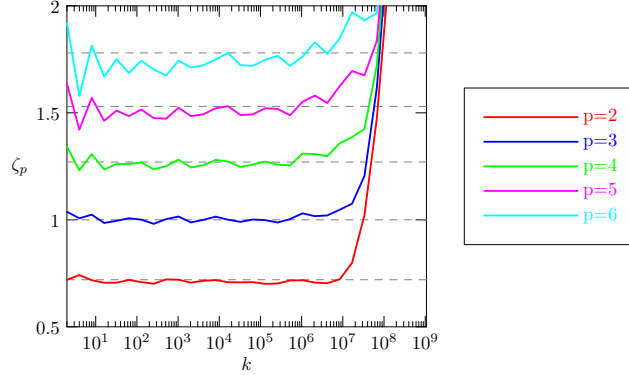


Figure 2.4: A comparison of structure-function exponents  $\zeta_p$ ,  $p = 2, \dots, 6$  (bottom to top) for the GOY model with experimental results.

the nonlinear transfer in the fluid. The energies of modes with wavenumbers higher than  $k_d$  drop precipitously, and do not as such contribute to the general cascade. This can be used to estimate the number of modes needed for a particular simulation. Kolmogorov's prediction was

$$k_d \sim \left( \frac{\nu^3}{\epsilon} \right)^{-\frac{1}{4}}. \quad (2.31)$$

Using the inertial-range scaling, we can write the Reynolds number as

$$R = \frac{LU}{\nu} \sim \frac{L(\epsilon L)^{\frac{1}{3}}}{\epsilon^{\frac{1}{3}} k_d^{-\frac{4}{3}}} = (k_d L)^{\frac{4}{3}}. \quad (2.32)$$

If we seek to resolve a range from the large scale  $L$  to the dissipation scale  $2\pi/k_d$ , we need roughly  $(k_d L)^3 = R^{9/4}$  modes for three-dimensional turbulence. The characteristic time scale  $\tau$ , which is the time needed for an eddy of size  $k_d^{-1}$  to be advected its width by the most active modes, is restricted to  $\tau \leq R^{-3/2} L/U$ , which is a further restriction beyond the  $R^{9/4}$  scaling for the number of modes required [Orszag 1970].

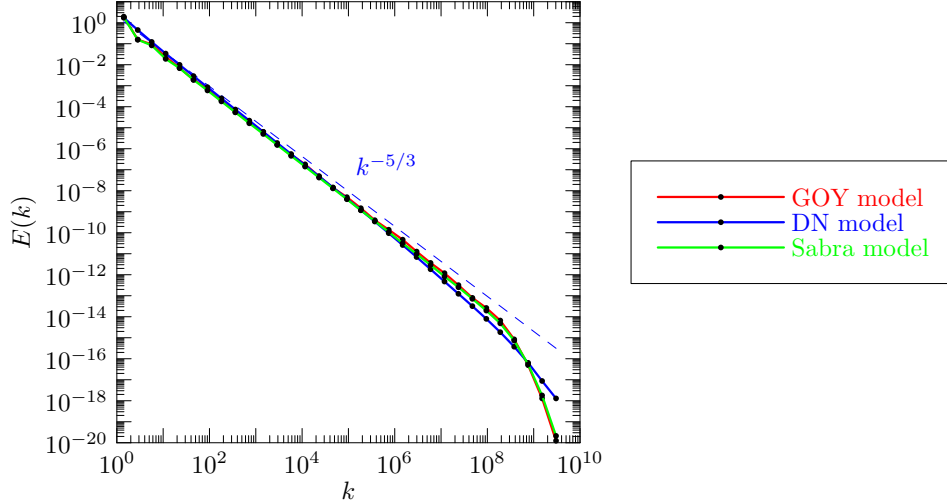


Figure 2.5: Comparison of DN, GOY, and Sabra turbulence.

While Kolmogorov’s four-fifths law has been confirmed to great precision in both numerical and physical experiments [Melander & Fabijonas 2006], the scaling of structure exponents  $S_p$  for  $p$  not equal to 3 are only approximately correct. The discrepancy is attributed to intermittency: the tendency of high-wavenumber excitations to be only partially space-filling. There are a number of theories that attempt to explain this, chief among which is the multi-fractal model [Frisch 1995].

Bowman *et al.* [2006] argued that the dissipation wavenumber should scale as

$$k_d \sim \nu^{1/(\frac{4}{3}-\delta)}, \quad (2.33)$$

where  $\delta = \zeta_2 - 2/3$  is the *second-order intermittency correction*. For example, they found  $k_d \sim \nu^{-0.7855 \pm 0.0005}$  in a study of GOY-model turbulence. The predictions of the multi-fractal model also differ from classic Kolmogorov theory with regards to the structure functions. In particular, Kolmogorov predicted

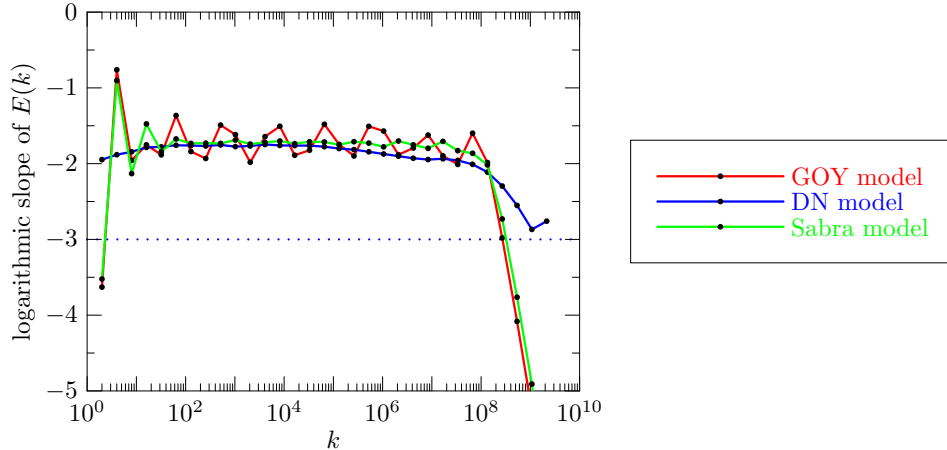


Figure 2.6: Logarithmic slopes for DN, GOY, Sabra turbulence.

that  $\zeta_p$  is proportional to  $p$ , whereas observations and the multi-fractal model indicate that  $\zeta_p$  is concave down.

One drawback of the DN model is that it lacks intermittency entirely [Bell & Nelkin 1977], at least for (uniform) coefficients  $a$  and  $b$  of opposite sign. The GOY model does exhibit intermittency for some values of the parameters  $\alpha$ ,  $\beta$ ,  $\gamma$ , and  $\lambda$ . In particular, the standard choice  $\lambda = 2$ ,  $\alpha = 1$ ,  $\beta = -1/2$ , and  $\gamma = -1/2$  preserves helicity and allows intermittent behaviour. Kadanoff *et al.* [1995] suggested that helicity preservation leads to unique intermittency corrections, but recently this was shown not to be the case [Bowman *et al.* 2006]. In addition to corrections owing to intermittency, Kolmogorov’s scaling has been modified to account for wavenumber “boundary conditions” at the forcing scale [Bowman 1996].

While the structure functions and energy spectra are important features of turbulence theory, they are not exhaustive tests. As a thought experiment, one could take the velocity field and randomise the phase at a point when the turbulence has reached a statistical steady state. While the energy spec-

trum would remain unchanged, any coherent structure would be eliminated [Farge 2006]. Since coherent structures are thought to play important roles in turbulence [McWilliams 1984], the correct prediction of the energy spectrum is a necessary but not sufficient test for the validity of a theory of turbulence.

# Chapter 3

## Equipartition

*In which we consider inviscid turbulence in the context of statistical mechanics.*

A system governed by the Navier–Stokes equation may be completely characterised by the vorticity field,  $\{\omega_{\mathbf{k}}, \mathbf{k} \in D\}$ , for some set  $D$ , called the *phase space*, which depends on the physical domain of the turbulence. The evolution of a system is a one-dimensional curve in this space. For physical systems, the phase space is an infinite-dimensional vector space. In computer simulations, we are only able to simulate finite-dimensional systems, which implies that the domain  $D$  must be bounded. We reproduce results in this chapter for the finite-dimensional case, most of which can be extended to the infinite-dimensional case.

We start with the vorticity formulation of the inviscid and unforced two-dimensional Navier–Stokes equation in Fourier space [Bowman *et al.* 1999],

$$\dot{\omega}_{\mathbf{k}} = \sum_{\mathbf{p}, \mathbf{q}} \frac{\epsilon_{\mathbf{k}\mathbf{p}\mathbf{q}}}{p^2} \omega_{\mathbf{p}}^* \omega_{\mathbf{q}}^*. \quad (3.1)$$

Here,  $\epsilon_{\mathbf{k}\mathbf{p}\mathbf{q}} \doteq (\hat{z} \cdot \mathbf{p} \times \mathbf{q}) \delta(\mathbf{k} + \mathbf{p} + \mathbf{q})$  and  $\mathbf{k}$ ,  $\mathbf{p}$ , and  $\mathbf{q}$  are wavevectors that come from a finite subset of  $\mathbb{Z}^2$ . We can write (3.1) as a noncanonical Hamiltonian system:

$$\dot{\omega}_{\mathbf{k}} = \sum_{\mathbf{q}} J_{\mathbf{k}\mathbf{q}} \frac{\partial H}{\partial \omega_{\mathbf{q}}}, \quad (3.2)$$

in which  $H = \frac{1}{2} \sum_{\mathbf{k}} |\omega_{\mathbf{k}}|^2 / k^2$  is the Hamiltonian and  $J_{\mathbf{k}\mathbf{q}} = \sum_{\mathbf{p}} \epsilon_{\mathbf{k}\mathbf{p}\mathbf{q}} \omega_{\mathbf{p}}^*$ . Note that  $J_{\mathbf{k}\mathbf{q}} = -J_{\mathbf{q}\mathbf{k}}$  owing to the antisymmetry of  $\epsilon_{\mathbf{k}\mathbf{p}\mathbf{q}}$  under interchange of any two indices. We take the derivative of (3.2) with respect to  $\omega_{\mathbf{k}}$  and obtain

$$\begin{aligned} \sum_{\mathbf{k}} \frac{\partial \dot{\omega}_{\mathbf{k}}}{\partial \omega_{\mathbf{k}}} &= \sum_{\mathbf{k}, \mathbf{q}} \frac{\partial J_{\mathbf{k}\mathbf{q}}}{\partial \omega_{\mathbf{k}}} + J_{\mathbf{k}\mathbf{q}} \frac{\partial^2 H}{\partial \omega_{\mathbf{k}} \partial \omega_{\mathbf{q}}} \\ &= \sum_{\mathbf{k}, \mathbf{q}} \epsilon_{\mathbf{k}(-\mathbf{k})\mathbf{q}} + \sum_{\mathbf{k}, \mathbf{q}} J_{\mathbf{k}\mathbf{q}} \frac{\partial^2 H}{\partial \omega_{\mathbf{k}} \partial \omega_{\mathbf{q}}} = 0, \end{aligned} \quad (3.3)$$

where the first sum vanishes because  $\epsilon_{\mathbf{k}(-\mathbf{k})\mathbf{q}} = \epsilon_{\mathbf{q}\mathbf{k}(-\mathbf{k})} = 0$  and the second term vanishes since it is the sum of the product of an antisymmetric and a symmetric factor. Equation (3.3) is known as a *Liouville theorem*, and implies that the system conserves volume in phase space.

The entropy of the system is

$$S(t) \doteq - \sum_i N_i \log N_i \quad (3.4)$$

where  $N_i$  is the number of modes in state  $i$ . This is constrained by the invariants of the system, energy and enstrophy. Let  $\epsilon_i$  and  $\xi_i$  be the energy and enstrophy of each mode in state  $i$ , respectively. If a system is ergodic, the *Gibbs H theorem* states that the equilibrium state of the system is the unique state that maximises the entropy of the system. Indeed, we expect the

entropy of a system to increase, not necessarily monotonically, until it reaches an equilibrium state where the entropy is constant and maximal. However, this extremisation must be subject to the constraints of energy and enstrophy conservation. In general, we may have many conserved quantities, which we label  $E_j \doteq \frac{1}{2} \sum_{\mathbf{k}} \sigma_{\mathbf{k}}^j |\omega_{\mathbf{k}}|^2$ , for certain functions  $\sigma_{\mathbf{k}}^j$ , where  $j = 1, \dots, n_c$ . Each of these provides a constraint  $E_j = \sum_i \epsilon_{i,j} N_i$ , where  $\epsilon_{i,j}$  is the amount of quantity  $E_j$  for each mode in state  $i$ . In addition, the total number of modes  $\sum_i N_i$  is constrained to be  $N$ . The equilibrium state will therefore minimise

$$\sum_i N_i \log N_i - \alpha_0 \left( N - \sum_i N_i \right) - \sum_j \alpha_j \left( E_j - \sum_i \epsilon_{i,j} N_i \right), \quad (3.5)$$

where the  $\alpha_j$  are Lagrange multipliers. On setting the derivative of (3.5) with respect to  $N_i$  to zero and solving for  $N_i$ , one obtains the *Gibbs distribution*

$$N_i = \exp \left( -1 - \alpha_0 - \sum_j \alpha_j \epsilon_{i,j} \right). \quad (3.6)$$

If there are  $N$  independent complex amplitudes  $\omega_{\mathbf{k}}$ , there will be  $2N$  degrees of freedom, which we arbitrarily label by  $\kappa = 1, 2, \dots, 2N$ . Let  $\Omega = (\omega_1, \dots, \omega_{2N})$  be a point in phase space. On denoting the state of mode  $\kappa$  at  $\Omega$  by  $i_\kappa$ , one can compute the probability that the system is in state  $\Omega$ :

$$P(\Omega) \propto \prod_{\kappa} N_{i_\kappa} \propto \exp \left( - \sum_{\kappa,j} \alpha_j \epsilon_{i_\kappa,j} \right) q = \exp \left( - \sum_j \alpha_j E_j \right), \quad (3.7)$$

where  $\alpha_j$  is determined by the initial conditions of the system. The expected

value for the energy in mode  $\mathbf{k}$  is therefore

$$\langle \omega_{\mathbf{k}}^{r2} \rangle = \langle \omega_{\mathbf{k}}^{i2} \rangle = \frac{\int \omega_{\mathbf{k}}^{r2} P(\Omega) d\omega_1 \dots d\omega_{2N}}{\int P(\Omega) d\omega_1 \dots d\omega_{2N}}, \quad (3.8)$$

where  $\omega_{\mathbf{k}} = \omega_{\mathbf{k}}^r + i\omega_{\mathbf{k}}^i$ . In two dimensions, the conserved quantities are energy, enstrophy, and other (nonquadratic) Casimir invariants associated with infinitesimal parcel rearrangement. Since we choose to work in a finite spectral domain we lose conservation of the Casimir invariants. Only the two quadratic invariants (energy and enstrophy) survive this spectral truncation, so  $\{\sigma_{\mathbf{k}}^i : i = 1, \dots, n_c\} = \{1/k^2, 1\}$ . Since  $\int_{-\infty}^{\infty} e^{-ax} dx = \sqrt{\pi/a}$ , one finds, on accounting for the Hermiticity condition  $\omega_{\mathbf{k}} = \omega_{-\mathbf{k}}^*$ , that

$$\langle |\omega_{\mathbf{k}}|^2 \rangle = \langle \omega_{\mathbf{k}}^{r2} \rangle + \langle \omega_{\mathbf{k}}^{i2} \rangle = \frac{1}{\alpha/k^2 + \beta} \quad (3.9)$$

for some constants  $\alpha$  and  $\beta$  that are determined by the total energy and enstrophy present in the initial conditions. On noting that  $E(k) \doteq 2\pi k \langle \frac{1}{2} |\omega_{\mathbf{k}}|^2 \rangle / k^2$ , we obtain the equipartition spectrum,

$$E(k) = \pi \frac{k}{\alpha + \beta k^2}. \quad (3.10)$$

Three-dimensional turbulence follows a similar argument, except that helicity is conserved, while enstrophy is not. Because helicity is not positive-semidefinite, it is not thought to play a role in the equipartition spectrum. Thus,  $\{\sigma_{\mathbf{k}}^i : i \in I\} = \{1\}$ , and the three-dimensional equipartition spectrum is

$$E(k) = 4\pi k^2 \frac{1}{k^2} \left\langle \frac{1}{2} |\omega_{\mathbf{k}}|^2 \right\rangle = \frac{2\pi k^2}{\alpha}. \quad (3.11)$$

Since the equations governing the DN, GOY, and Sabra models of turbulence do not explicitly depend on  $u_n$  but rather on the complex conjugate of  $u_n$ , a Liouville's theorem follows immediately. For parameters mimicking 3D turbulence, the only positive-semidefinite invariant of these models is energy, so we then expect an equipartition of the modal energies  $\langle |u_n|^2 \rangle$ . Thus

$$E(k_n) = \frac{1}{2} \frac{\langle |u_n|^2 \rangle}{k_{n+1} - k_n} \sim k_n^{-1}. \quad (3.12)$$

When both energy and enstrophy are conserved, as can be the case for the GOY and Sabra models under suitable coefficient choices,

$$E(k_n) \sim \frac{1}{\alpha k_n + \beta k_n^3}. \quad (3.13)$$

This is different than the spectrum for inviscid unforced two-dimensional turbulence by a factor of  $k^2$  due to geometric factors.

As a final note, we emphasise that these results were attained for a system with a finite number of modes; they are not applicable to systems with infinite degrees of freedom.

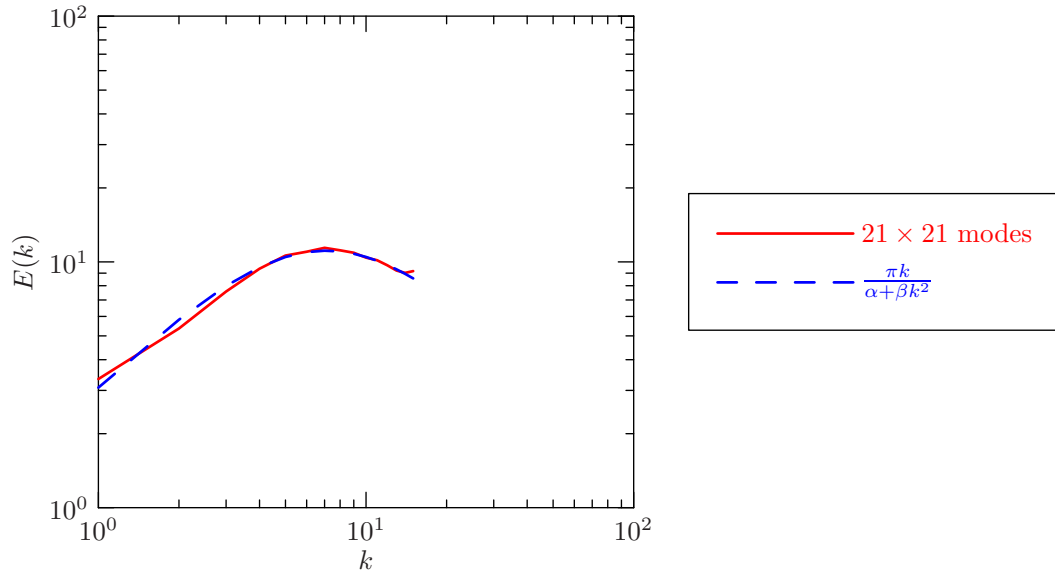


Figure 3.1: Equipartition energy spectrum of two-dimensional Navier–Stokes turbulence.

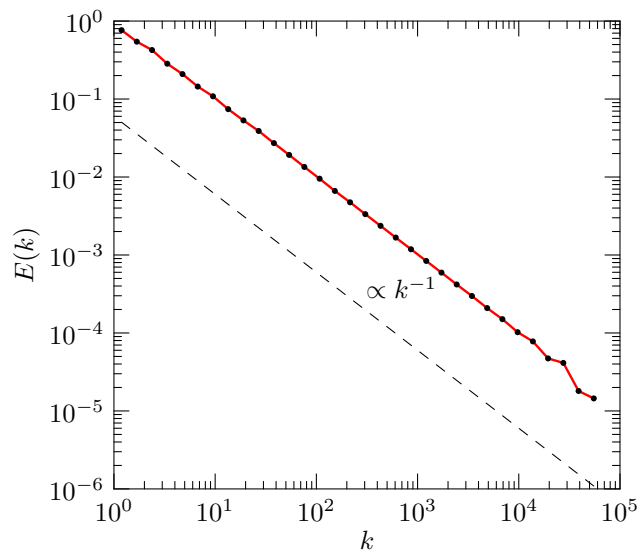


Figure 3.2: Equipartition energy spectrum of “3D” GOY turbulence.

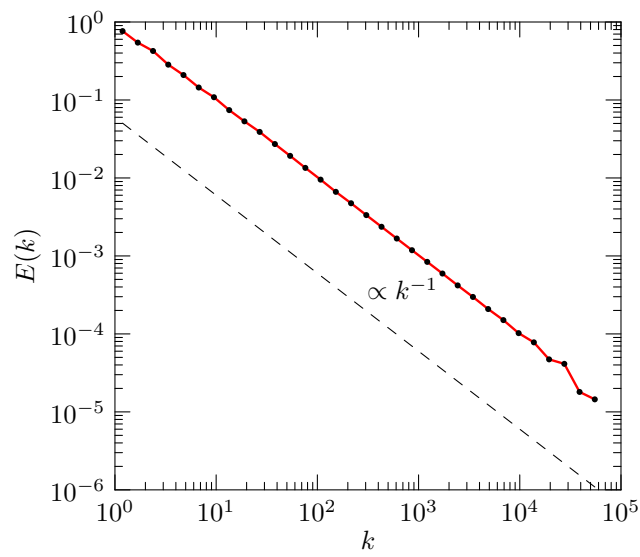


Figure 3.3: Equipartition energy spectrum of DN turbulence.

# Chapter 4

## Spectral Reduction

*In which we discuss a method for simulating turbulence.*

Full two- or three-dimensional turbulent simulations at high Reynolds numbers will remain out of our reach for the foreseeable future. While the situation at present may be grim, there is hope based “on the observation that the problem is one of approximation” [Orszag 1970]. The majority of the modes in turbulent simulations are concentrated at high wavenumbers around the dissipation range, but these modes contain a minority of the energy in the system. Furthermore, we are often not interested in the exact behaviour at these small scales, for which we typically do not even have observational data with which to initialise our simulations.

The method of *spectral reduction* [Bowman *et al.* 1999] takes into account the disparity between the number of degrees of freedom and the physical importance associated with each scale. In this method, the equations of turbulence are solved on a coarse mesh in Fourier space, possibly of variable resolution. Spectral reduction was originally formulated for two-dimensional Navier–Stokes turbulence.

## 4.A Spectral reduction of Navier–Stokes turbulence

The application of spectral reduction to two-dimensional turbulence is made convenient by the fact that the velocity field can be calculated using just one scalar variable, the vorticity. If we take the vorticity formulation of (1.1) in two dimensions (1.11), and take the Fourier transform, we get

$$\frac{\partial}{\partial t}\omega_{\mathbf{k}} + \nu_{\mathbf{k}}\omega_{\mathbf{k}} = \int \int \frac{\epsilon_{\mathbf{k}\mathbf{p}\mathbf{q}}}{p^2} \omega_{\mathbf{p}}^* \omega_{\mathbf{q}}^* d\mathbf{p} d\mathbf{q} + F_{\mathbf{k}}, \quad (4.1)$$

where

$$\epsilon_{\mathbf{k}\mathbf{p}\mathbf{q}} \doteq (\hat{\mathbf{z}} \cdot \mathbf{p} \times \mathbf{q}) \delta(\mathbf{k} + \mathbf{p} + \mathbf{q}) \quad (4.2)$$

is antisymmetric under interchange of any two indices. In a square-periodic domain, the integrals in (4.1) may be replaced by summation. In this case, the modes  $\mathbf{k}$  are restricted to  $\mathbb{Z}^2$ . The mode  $\omega_{\mathbf{0}}$  is affected only by  $F_{\mathbf{0}}$ , and as such is not usually calculated as part of the simulation. Also, the Hermiticity condition,  $\omega_{-\mathbf{k}} = \omega_{\mathbf{k}}^*$ , which guarantees that the velocity field be real-valued, eliminates the need to explicitly calculate half of the modes. Let  $d$  be the set of wavevectors associated with the active modes. We take  $d$  to be bounded, as it must be if we wish to solve the system on a computer.

The goal of spectral reduction is to approximate (4.1) on a grid  $D$  that has fewer points than  $d$ . To each cell of  $D$ , we assign a characteristic wavevector  $\mathbf{K} \in \mathbb{R}^2$ . Each mesh point  $\mathbf{K}$  is associated with a number of fine-mesh wavevectors from  $d$ . We label this set  $V_{\mathbf{K}} = \{\mathbf{k}_{\mathbf{K}_1}, \dots, \mathbf{k}_{\mathbf{K}_{\ell(\mathbf{K})}}\} \subset d$ . These

modes are chosen so that the coarse-mesh wavevector  $\mathbf{K}$  is representative of the wavevectors  $V_{\mathbf{K}}$ , i.e. the wavevectors in  $V_{\mathbf{K}}$  are close to  $\mathbf{K}$ .

To each wavevector  $\mathbf{K}$  we associate the variable

$$\Omega_{\mathbf{K}} \doteq \frac{1}{|V_{\mathbf{K}}|} \sum_{\mathbf{k} \in V_{\mathbf{K}}} \omega_{\mathbf{k}}, \quad (4.3)$$

where  $|V_{\mathbf{K}}|$  is the size of the set  $V_{\mathbf{K}}$ . We can use this prescription to calculate the evolution of  $\Omega_{\mathbf{K}}$ , which is

$$\frac{\partial \Omega_{\mathbf{K}}}{\partial t} + \langle \nu_{\mathbf{k}} \omega_{\mathbf{k}} \rangle_{\mathbf{K}} = \sum_{\mathbf{P}, \mathbf{Q} \in D} |V_{\mathbf{P}}| |V_{\mathbf{Q}}| \left\langle \frac{\epsilon_{\mathbf{k}pq}}{q^2} \omega_{\mathbf{p}}^* \omega_{\mathbf{q}}^* \right\rangle_{\mathbf{K}PQ} + \langle F_{\mathbf{k}} \rangle_{\mathbf{K}}, \quad (4.4)$$

where the notation  $\langle f \rangle_{\mathbf{K}_1, \dots, \mathbf{K}_\ell}$  denotes the mean value of  $f$  over the bins  $\mathbf{K}_1, \dots, \mathbf{K}_\ell$ . We close the equation by approximating  $\omega_{\mathbf{k}}$  with  $\Omega_{\mathbf{K}}$ :

$$\frac{\partial \Omega_{\mathbf{K}}}{\partial t} + \langle \nu_{\mathbf{k}} \rangle_{\mathbf{K}} \Omega_{\mathbf{K}} = \sum_{\mathbf{P}, \mathbf{Q} \in D} |V_{\mathbf{P}}| |V_{\mathbf{Q}}| \left\langle \frac{\epsilon_{\mathbf{k}pq}}{q^2} \right\rangle_{\mathbf{K}PQ} \Omega_{\mathbf{P}}^* \Omega_{\mathbf{Q}}^* + \langle F_{\mathbf{k}} \rangle_{\mathbf{K}}. \quad (4.5)$$

While (4.4) is an exact prescription for  $\partial \Omega_{\mathbf{K}} / \partial t$ , the interaction coefficient

$$\left\langle \frac{\epsilon_{\mathbf{k}pq}}{q^2} \right\rangle_{\mathbf{K}PQ} \quad (4.6)$$

in (4.5) is not antisymmetric under the transformation  $\mathbf{K} \leftrightarrow \mathbf{P}$ , which breaks enstrophy conservation. In order to restore this symmetry, one uses the modified interaction coefficient

$$\frac{\langle \epsilon_{\mathbf{k}pq} \rangle_{\mathbf{K}PQ}}{Q^2}. \quad (4.7)$$

The resulting equation,

$$\frac{\partial \Omega_{\mathbf{K}}}{\partial t} + \langle \nu_{\mathbf{k}} \rangle_{\mathbf{K}} \Omega_{\mathbf{k}} = \sum_{\mathbf{P}, \mathbf{Q} \in D} |V_{\mathbf{P}}| |V_{\mathbf{Q}}| \frac{\langle \epsilon_{\mathbf{k}pq} \rangle_{\mathbf{K}PQ}}{Q^2} \Omega_{\mathbf{P}}^* \Omega_{\mathbf{Q}}^* + \langle F_{\mathbf{k}} \rangle_{\mathbf{K}}, \quad (4.8)$$

conserves both energy and enstrophy in the absence of viscosity and forcing.

One particularly advantageous coarse-mesh choice is the set of radially spaced bins illustrated in Fig. 4.1, which reach high wavenumbers and have high resolution near the origin while using very few modes. In one simulation, Bowman *et al.* were able to mimic the energy spectrum of forced-dissipative turbulence on a fine mesh of  $683 \times 683$  dealiased modes using only a few dozen radially spaced mesh points [Bowman *et al.* 1996].

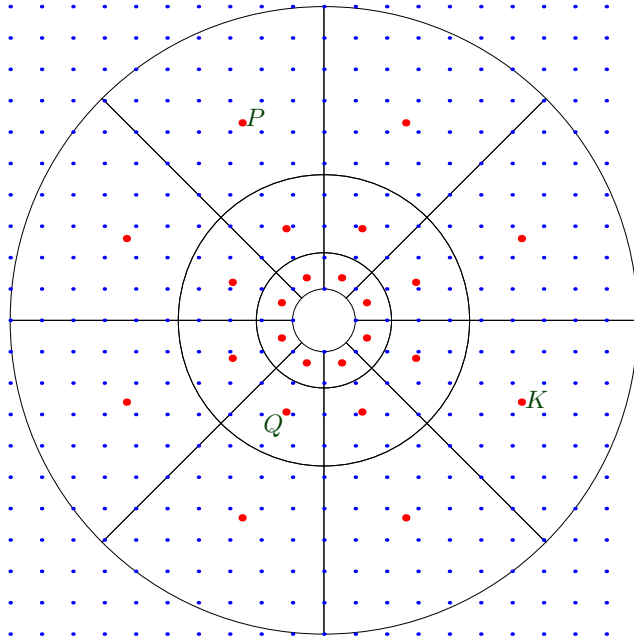


Figure 4.1: Polar wavenumber bin geometry.

However, this method of spectral reduction requires modification to reproduce equipartition spectra. If the bins are not uniformly spaced (as in radial

spacing, for example), time needs to be rescaled in (4.8) by the bin area. That is,

$$\frac{|V_{\min}|}{|V_{\mathbf{K}}|} \frac{\partial \Omega_{\mathbf{K}}}{\partial t} + \langle \nu_k \rangle_{\mathbf{K}} \Omega_{\mathbf{k}} = \sum_{P, Q} |V_P| |V_Q| \frac{\langle \epsilon_{kpq} \rangle_{\mathbf{K}PQ}}{Q^2} \Omega_P^* \Omega_Q^* + \langle F_k \rangle_{\mathbf{K}}, \quad (4.9)$$

where  $|V_{\min}|$  is the minimum bin size. Under this transformation, (4.9) is able to reproduce the two-dimensional equipartition spectrum discussed in Chapter 3. Unfortunately, the resulting system is very stiff if the modes are radially spaced, where  $|V_{\mathbf{K}}| \sim K^2$ , which forces the time step to be very small. The efficient numerical approximation of this equation is an open problem [Bowman *et al.* 2001]. Furthermore, energy is not conserved when time is rescaled.

## 4.B Spectral reduction of shell model turbulence

We return to shell models of turbulence for insight. Shell models are computed on very simple meshes and have fewer inter-modal interactions than the Navier–Stokes equation. Both these facts greatly simplify spectral reduction. We begin with the spectral reduction of the GOY model.

The evolution equation for the GOY model is given in (1.20), where the wavenumbers are  $k_n$  for  $n \in \mathbb{N}$ . We define the first-order spectrally reduced (coarse-grid) mode to be

$$u_n^{(1)} = \frac{u_{2n} + \sigma_n^{(0)*} u_{2n+1}}{1 + |\sigma_n^{(0)}|^2}, \quad (4.10)$$

where  $\sigma_n^{(0)} = u_{2n+1}/u_{2n}$  is the ratio between adjacent modes. This is a modification of the procedure in [Bowman *et al.* 2001], where  $\sigma_n^{(0)}$  was taken to be unity. If we knew  $\sigma_n^{(0)}$  exactly, we would of course have exact formulae for  $u_{2n}$  and  $u_{2n+1}$  in terms of  $u_n^{(1)}$ , namely  $u_{2n} = u_n^{(1)}$ , and  $u_{2n+1} = \sigma_n^{(0)} u_n^{(1)}$ . If we approximate  $\sigma_n^{(0)}$  by the constants  $\left(\langle |u_{n+1}^{(1)}|^2 \rangle / \langle |u_n^{(1)}|^2 \rangle\right)^{1/4}$ , the evolution equation for  $u_n^{(1)}$  becomes

$$\begin{aligned} \frac{du_n^{(1)}}{dt} = & -\nu k_{2n}^2 \frac{1 + \sigma_n^{(0)*} \lambda^2}{1 + |\sigma_n^{(0)}|^2} u_n^{(1)} + \frac{F_n + \sigma_n^{(0)*} F_{n+1}}{1 + |\sigma_n^{(0)}|^2} \\ & + \frac{1}{1 + |\sigma_n^{(0)}|^2} i k_{2n} \left[ \sigma_{n-1}^{(0)} \frac{\gamma}{\lambda^2} u_{n-1}^{(1)2} + \sigma_n^{(0)} (\alpha + \beta) u_n^{(1)} u_{n+1}^{(1)} \right. \\ & \left. + \sigma_{n-1}^{(0)} \sigma_n^{(0)} \left( \frac{\beta}{\lambda} + \frac{\gamma}{\lambda} \right) u_{n-1}^{(1)} u_n^{(1)} + \lambda \alpha \sigma_n^{(0)} \sigma_{n+1}^{(0)} u_{n+1}^{(1)2} \right]^* . \end{aligned} \quad (4.11)$$

The coarse-grained energy  $E = \frac{1}{2} \sum_n |u_n^{(1)}|^2 (1 + |\sigma_n^{(0)}|^2)$  is conserved in the absence of forcing and viscosity if the original model conserved energy and  $\sigma_n^{(0)}$  is constant with respect to time. Other quadratic invariants (i.e. helicity or enstrophy) are lost.

If  $\alpha + \beta + \gamma = 0$ , i.e. the underlying GOY model conserves energy, (4.11) is the DN model (1.18) with parameters given by [Eckhardt 2004]

$$\begin{aligned} u_n^{(1)} = & \frac{u_{2n} + \sigma_n^{(0)*} u_{2n+1}}{1 + |\sigma_n^{(0)}|^2}, \quad a_n^{(1)} = \frac{\gamma}{\lambda^2} \left( \frac{\sigma_{n-1}^{(0)}}{1 + |\sigma_n^{(0)}|^2} \right), \quad b_n^{(1)} = \frac{-\alpha}{\lambda} \left( \frac{\sigma_{n-1}^{(0)} \sigma_n^{(0)}}{1 + |\sigma_n^{(0)}|^2} \right), \\ \lambda^{(1)} = & \lambda^2, \quad \nu_n^{(1)} = \nu \frac{1 + |\sigma_n^{(0)}|^2 \lambda^2}{1 + |\sigma_n^{(0)}|^2}, \quad \text{and} \quad F_n^{(1)} = \frac{F_n + \sigma_n^{(0)*} F_{n+1}}{1 + |\sigma_n^{(0)}|^2}. \end{aligned} \quad (4.12)$$

It is easy to see that spectral reduction of the GOY model should produce the DN model if we consider Fig. 4.2. Since interactions in the GOY model are next-nearest-neighbour, a radix-two scheme, such as spectral reduction, produces binned modes with interactions that are nearest-neighbour between bins.

The resulting system is energy-conserving, has a nonlinearity that is quadratic in the complex-conjugate of the velocity field, and has nearest-neighbour interactions. In other words, it is the DN model.

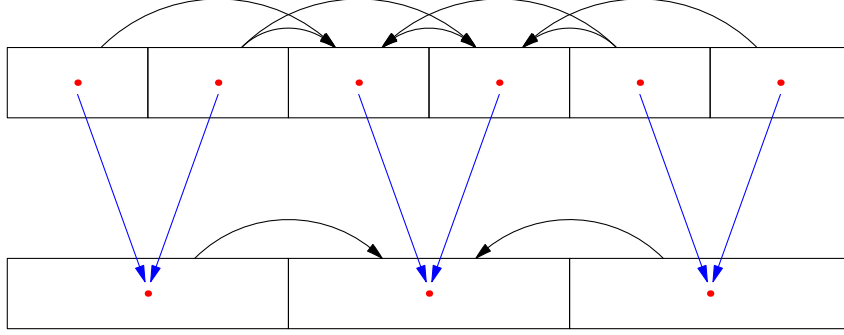


Figure 4.2: Spectral reduction of the GOY model showing emergence of nearest-neighbour interactions.

If we apply the method of spectral reduction again, setting

$$u_n^{(2)} = \frac{u_{2n}^{(1)} + \sigma_n^{(1)*} u_{2n+1}^{(1)}}{1 + |\sigma_n^{(1)}|^2}, \quad \sigma_n^{(1)} = \left( \frac{\langle |u_{n+1}^{(2)}|^2 \rangle}{\langle |u_n^{(2)}|^2 \rangle} \right)^{1/4}, \quad (4.13)$$

the governing equation becomes

$$\begin{aligned} \frac{du_n^{(2)}}{dt} &= \frac{1}{1 + |\sigma_n^{(1)}|^2} \left( \frac{du_{2n}^{(1)}}{dt} + \sigma_n^{(1)*} \frac{du_{2n+1}^{(1)}}{dt} \right) \\ &= ik_{2n} \left( a_n^{(2)} u_{n-1}^{(2)2} - \lambda^{(2)} a_{n+1}^{(2)} u_n^{(2)} u_{n+1}^{(2)} \right)^* \\ &\quad \times \left( b_n^{(2)} u_{n-1}^{(2)} u_n^{(2)} - \lambda^{(2)} b_{n+1}^{(2)} u_{n+1}^{(2)2} \right)^* - \nu_n^{(2)} k_{2n}^2 u_n^{(2)} + F_n^{(2)}, \end{aligned} \quad (4.14)$$

which is the DN model with coefficients given by (4.15) with  $\ell = 1$ . Subsequent applications of the method of spectral reduction leave the form of the equation

similarly unchanged, remapping the coefficients as per (4.15) [Eckhardt 2004].

$$\begin{aligned}
u_n^{(\ell)} &\rightarrow u_n^{(\ell+1)}, & a_n^{(\ell+1)} &= \frac{\sigma_n^{(\ell)2}}{1 + |\sigma_n^{(\ell)}|^2} a_n^{(\ell)}, & b_n^{(\ell+1)} &= \frac{\sigma_{n-1}^{(\ell)}}{1 + |\sigma_n^{(\ell)}|^2} b_n^{(\ell)}, & (4.15) \\
\nu_n^{(\ell+1)} &= \nu_n^{(\ell)} \frac{1 + \lambda^{(\ell)2} |\sigma_n^{(\ell)}|^2}{1 + |\sigma_n^{(\ell)}|^2}, & \lambda^{(\ell+1)} &= \lambda^{(\ell)2}, & \text{and} & F_n^{(\ell+1)} &= \frac{F_n^{(\ell)} + \sigma_n^{(\ell)*} F_{n+1}^{(\ell)}}{1 + |\sigma_n^{(\ell)}|^2}.
\end{aligned}$$

The energy for this system,  $E = \sum_n u_n^{(\ell+1)} \prod_{j=0}^i (1 + |\sigma_n^{(j)}|^2)$  is conserved by the nonlinearity when the  $\sigma$ s are constant. In practise, we close the equations using the approximation

$$\sigma_n^{(\ell)} = \left( \frac{\left\langle \left| u_{n+1}^{(\ell+1)} \right|^2 \right\rangle}{\left\langle \left| u_n^{(\ell+1)} \right|^2 \right\rangle} \right)^{1/4} \quad (4.16)$$

in numerical simulations. The interpolation is further smoothed by using a cubic spline on the moments  $\left\langle \left| u_n^{(\ell+1)} \right|^2 \right\rangle$ . This approximation sets  $\sigma_n^{(\ell)}$  to be real, but avoids the numerical instabilities and complex square roots encountered in the more straightforward approximation  $\sigma_n^{(\ell)} = \sqrt{u_{n+1}^{(\ell+1)} / u_n^{(\ell+1)}}$ , which is very sensitive to fluctuations in the velocity field.

The spectrally reduced shell models will only attain the correct equipartition spectrum if all the bins are of equal size. If, for example, we choose to bin some modes and not others, the correct equipartition spectrum will only be reached if we also rescale time by the relative bin sizes. Unfortunately, rescaling time by the relative bin size breaks energy conservation.

The governing equation for the Sabra model contains a mixture of velocities and complex conjugates of velocities, which makes the application of the method of spectral reduction to the Sabra model somewhat more arduous.

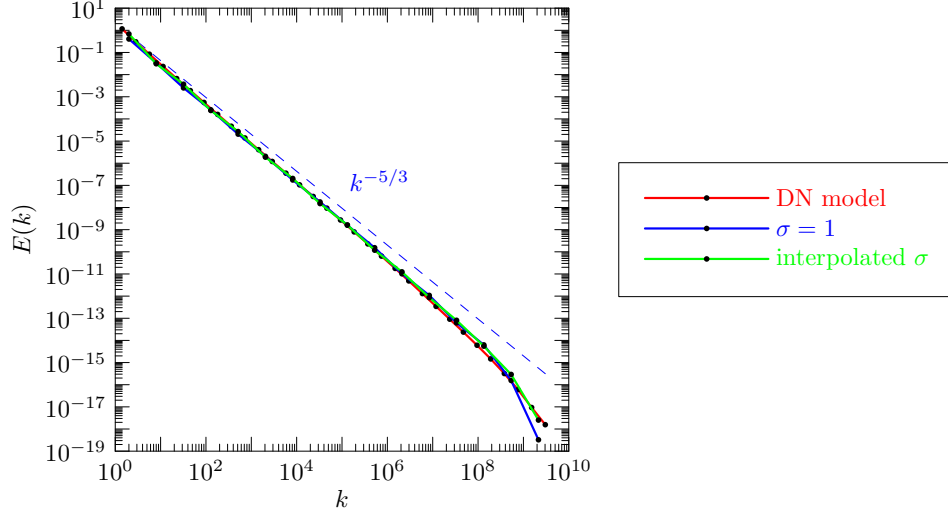


Figure 4.3: Energy spectra computed with interpolated spectral reduction.

Using the substitution given in equation 4.10, the governing equation of the spectrally reduced mode is

$$\begin{aligned} \frac{du_n^{(1)}}{dt} = \frac{ik_{2n}}{1 + |\sigma_n^{(0)}|^2} & \left( -\frac{\gamma}{\lambda^2} \sigma_{n-1}^{(0)} u_{n-1}^{(1)2} - \frac{\gamma}{\lambda} \sigma_n^{(0)*} \sigma_{n-1}^{(0)} u_{n-1}^{(1)} u_n^{(1)*} + \frac{\beta}{\lambda} \sigma_{n-1}^{(0)*} \sigma_n^{(0)} u_{n-1}^{(1)*} u_n^{(1)} \right. \\ & \left. + (\alpha + \beta) \sigma_n^{(0)*} u_n^{(1)*} u_{n+1}^{(1)} + \alpha \lambda \sigma_n^{(0)*} \sigma_{n+1}^{(0)*} u_{n+1}^{(1)} u_{n+1}^{(1)*} \right), \end{aligned} \quad (4.17)$$

where the viscous and force terms change as in the spectral reduction of the GOY model, given by (4.12). This new model is nearest-neighbour, and conserves energy whenever  $\alpha + \beta + \gamma = 0$ , as in the GOY and Sabra models. Another application of spectral reduction yields models with seven source terms. Thankfully, the form of the governing equation is invariant upon further applications of spectral reduction. Unfortunately, the spectrally reduced Sabra model behaves differently than the Sabra model, attaining, for example, an  $E(k) \sim k^{-2.25}$  equipartition spectrum instead of  $E(k) \sim k^{-1}$ .

In the following chapters, we shall restrict ourselves then to the GOY

and DN models of turbulence because the spectrally reduced GOY model has similar behaviour to the GOY model. While spectral reduction captures the overall behaviour of the shell models, we would like to overcome the condition that bin size be constant. Unfortunately, we experience the same problem with variable bin size in shell models of turbulence as we did in Navier–Stokes turbulence: the system does not reach the equilibrium that we predicted in Chapter (3), but instead has a discontinuity in  $E(k)$  between bins of different sizes. While this can be fixed by rescaling time by the bin size, this increases the stiffness of the system greatly and breaks energy conservation. Both of these problems are solved by using the multi-spectral method.

# Chapter 5

## The Multi-Spectral Method

*In which we introduce and develop a new computational method for turbulence.*

In this chapter, we propose a multi-spectral method as a computational technique for solving partial differential equations with variable resolution in Fourier space. It is designed for hyperbolic problems, for which multi-grid methods [[Briggs 1987], [Bramble 1993], [Hackbusch 1985]] are not generally applicable [Ames 1977].

In particular, we can choose to have high resolution at the large scales and low resolution at the small scales. In the models of turbulence we have discussed, external forcing is active at large scales, the large scales contain a majority of the energy, and we are often most interested physically in the large scales; for instance, it is the large scales that tell us which path a hurricane will take. However, we must also resolve very small scales in order to remove energy from the system in the dissipation range. Because we are not as concerned with the exact behaviour at the small scales, we can choose to use a low resolution grid at high wavenumbers.

## 5.A Other approximations

A common solution to the problem of separation of scales is to increase the viscosity so that the dissipation scale is large enough that we may model the system in a straightforward fashion. This may be accomplished by simply increasing  $\nu$ , which decreases the dissipation wavenumber  $k_d$ . Since turbulence can, to some extent, be characterised by the Reynolds number, arbitrarily setting  $\nu$  to match the computer instead of the physical system is not satisfying. Another method of increasing the effect of viscosity is to increase the degree of the Laplacian, which is called *hyperviscosity*. A linear term of the form  $\nu_h \nabla^{2h} \mathbf{u}_k$  for  $h \geq 1$  will decrease the dissipation wavenumber as  $h$  is increased (adjusting  $\nu_h$  to keep the total dissipation constant). However, hyperviscosity can introduce *bottlenecks* in the small-scale energy spectrum and distort the inertial range [Tran & Bowman 2003]. Another alternative is to introduce a Heaviside function viscosity at the small scales, which allows one to remove energy at the small scales. While this is useful in situations where one is interested solely in the large-scale dynamics, it could also greatly contaminate the inertial range. Despite these drawbacks, increasing viscosity remains a mainstay of turbulent simulations, owing to its simplicity and heuristically reasonable results at large scales in some cases.

There have been, of course, other attempts to simplify simulations of turbulence, such as the Smagorinsky model, the  $K - \epsilon$  model, and large-eddy simulations [Frisch 1995], [Basu & Porté-Agel 2005], [Dubos 2003]. In these models, the transfer of energy from the small scales to the large scales (the *back-scatter*) is removed, providing energy transfer only from large scales to small scales. While the energy does typically move from the large scales to the

small scales, it is increasingly thought that back-scatter plays an important role in turbulence [Piomelli *et al.* 1991] and should not be neglected.

If one is only interested in calculating the evolution of statistical moments, one option is to construct a *statistical closure* (e.g. see Orszag [1977], Bowman [1992], Bowman *et al.* [1993]). Consider (3.1), the two-dimensional Fourier-transformed vorticity formulation of the Navier–Stokes equation, for which we take the real case and represent in schematic form as

$$\frac{\partial \omega}{\partial t} + \nu \omega = M \omega \omega. \quad (5.1)$$

The evolution of the second order moment is governed by the equation

$$\begin{aligned} \frac{\partial}{\partial t} \langle \omega \omega \rangle &= 2 \left\langle \omega \frac{\partial \omega}{\partial t} \right\rangle \\ &= -2\nu \langle \omega \rangle + 2M \langle \omega \omega \omega \rangle. \end{aligned} \quad (5.2)$$

So, in order to determine the evolution of a second-order moment, we must know a third-order moment, and so on. To break this endless chain of dependence, one must introduce an approximation [Orszag 1970], [Orszag 1977]. For example, the fourth-order moment could be approximated as a sum of products of second-order moments. Such an approximation is called *quasinormal*. Unfortunately, the quasinormal approximation can lead to negative energies, which is unphysical. Other closure approximations, such as the *eddy-damped quasinormal Markovian* (EDQNM) closure [Orszag 1977] and the *test field model* [Kraichnan 1972] can also predict negative energies [[Bowman 1992], [Bowman *et al.* 1993], [Bowman & Krommes 1997]]. The *realisable Markovian closure* [Bowman *et al.* 1993] and the *realisable test field model*

[Bowman & Krommes 1997] solve the problem of negative energies. However, closure approximations *only* predict moments; they do not provide information about the underlying velocity field.

## 5.B The time-scale disparity

In both the Fourier-space representation of the Navier–Stokes equation and the governing equations of shell models of turbulence, the nonlinear part of the source term is proportional to the wavenumber. We should then expect the small scales, which have high wavenumbers, to evolve more quickly than the large scales. In fact, the slow evolution of the large scales is a common complaint in turbulence research because simulations must be run for an extraordinarily long time before the large scales reach equilibrium.

This time-scale disparity may be measured more easily for inviscid, unforced systems. In Chapter (3), we were able to predict the final spectrum for such systems. These systems evolve to a statistically steady state for which we are able to calculate  $E(k)$  based on the initial conditions. The time that it takes a mode  $u_k$  in GOY turbulence to approach equipartition (Fig. 5.1) is approximately of the form  $A - B \log k$  for modes with wavenumber less than the median wavenumber, and is roughly constant for modes with wavenumber greater than the median.

## 5.C The multi-spectral method

The separation of time scales in turbulence is reminiscent of the separation of time scales that lies at the heart of the multi-grid method [Ames 1977]. Owing

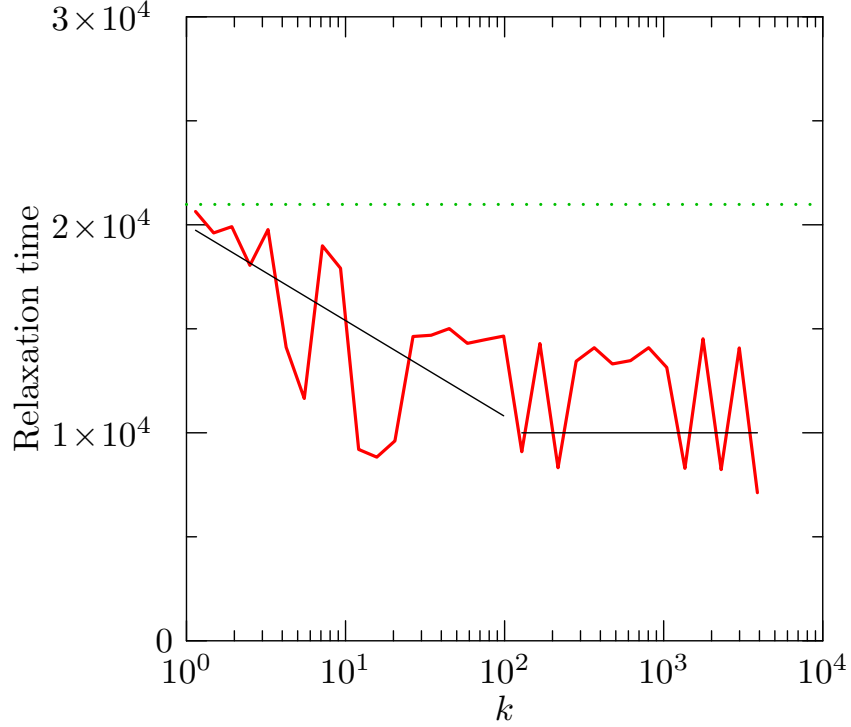


Figure 5.1: Relaxation time to equipartition for the GOY model.

to the presence of characteristics in the Euler equation, multi-grid methods have not been successfully applied to the Navier–Stokes equation. The *multi-spectral method* takes inspiration from multi-grid methods, but is set in Fourier space, while multi-grid methods are set in  $x$  space. We begin with two grids and a shell model.

The governing equation of a general shell model has the form

$$\left(\frac{d}{dt} + \nu k_n^2\right) u_n = ik_n \sum_{\ell, m} A_{\ell, m} u_\ell^* u_m^* + F_n, \quad (5.3)$$

where  $\nu$  is the coefficient of linear viscosity,  $F_n$  is an external force, and  $A_{\ell, m}$  are interaction coefficients. The complex-valued velocities  $u_n$  are associated with the wavenumber  $k_n = k_0 \lambda^n$ , for  $n = 0, \dots, N - 1$ . We would like to

simulate this model on a set of two grids, one with high resolution at low wavenumbers, and another with low resolution at high wavenumber.

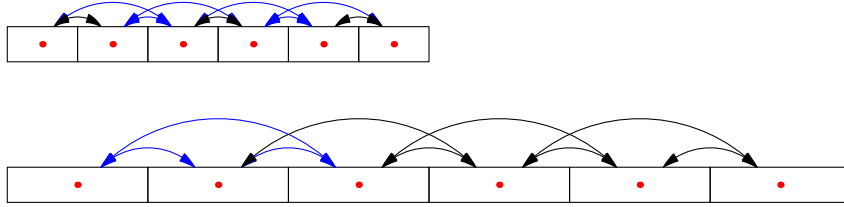


Figure 5.2: Arrangement of grids for the multi-spectral method, showing interactions for a general shell model.

The configuration we choose has overlapping grids, as shown in Fig. 5.2. The two grids have  $N_1$  and  $N_2$  modes, which need not be equal. The grids are arranged with low wavenumbers to the left and high wavenumbers to the right. The first grid has higher resolution and is limited to small wavenumbers. The second grid has lower resolution and thus covers a larger range of Fourier space per mode. We call these the *fine grid* and *coarse grid*, respectively. In this particular choice of grids, the coarse grid has twice the wavenumber spacing of the fine grid, so we call this a radix-two scheme and denote the binning factor  $\Delta = 2$ . The arrows represent interactions between modes. Clearly, some regions of Fourier space interact through both the fine grid and coarse grid. We call such interactions *redundant*, and they are shown drawn in blue. While these interactions are indeed important, they should not be calculated twice. In such situations, we choose to keep the interactions on the fine grid, eliminating them on the coarse grid. This result is shown in Fig. 5.3.

We label the modes on the fine grid  $u_n^{(1)}$ , for  $n = 1, \dots, N_1$  and the modes on the coarse grid  $u_n^{(2)}$ , for  $n = 1, \dots, N_2$ . Let the first mode on the coarse grid that is not part of the overlap be denoted  $u_{\frac{N_2}{2}}^{(2)}$ . The energy of the system

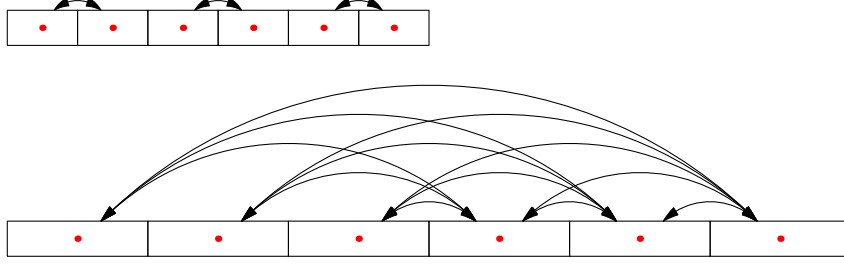


Figure 5.3: Arrangement of grids for the multi-spectral method, showing non-redundant interactions for a general shell model.

is

$$E = \frac{1}{2} \sum_{n=1}^{N_1} |u_n^{(1)}|^2 + \frac{1}{2} \sum_{m=\widehat{N}_2}^{N_2} |u_m^{(2)}|^2 \Delta. \quad (5.4)$$

In other words, we take the energy to be the sum of the energies of all the modes, multiplied by the size of the mode's bin relative to a fine bin. In the case where modes from different grids cover the same region of Fourier space, we choose the mode from the fine grid. We call such modes the *visible modes* of the system.

The DN model, introduced in Section 1.B.1, has the governing equation

$$\frac{\partial u_n}{\partial t} + \nu k_n^2 u_n = ik_n (a_n u_{n-1}^2 - \lambda a_{n+1} u_n u_{n+1} + b_n u_{n-1} u_n - \lambda b_{n+1} u_{n+1}^2)^* + F_n. \quad (5.5)$$

Since the interactions are nearest-neighbour, this is a particularly simple model to work with. Only one mode in the overlapping section of the coarse grid needs to be kept, as all others are redundant. The remaining interactions are shown in Fig. 5.4. We remind the reader of the fact that the GOY model reduces to the DN model upon the application of spectral reduction. Owing to the

simplicity of the DN model under spectral reduction, we will use it throughout this section.

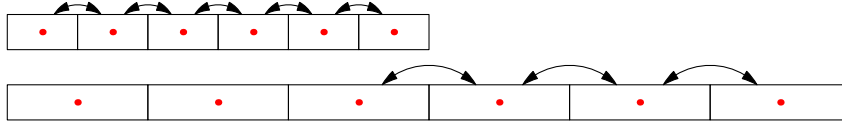


Figure 5.4: The multi-spectrum grid for the DN model showing all non-redundant interactions.

This system separates the interactions at large scales from the interactions at small scales. However, the two grids do need to interact; while there is some separation between scales, they are not totally unrelated. In particular, the systems should not drift apart as they are advanced in time. To this purpose we develop projection and prolongation operators between grids.

## 5.D Projection and prolongation

The projection operator transfers information from the fine grid to the coarse grid. The prolongation operator transfers information in the opposite direction. Since the fine and coarse grids overlap, we require that they at least approximately agree on the velocities of the model where they overlap. In particular, the projection and prolongation operators should preserve the invariants of the system both globally and locally. Further, the projection and prolongation operators should act locally in Fourier space to avoid introducing an anomalous transport of energy between scales.

Generally (e.g. in the DN model), the only invariant that we need concern ourselves with is the energy. This modal energy is  $\frac{1}{2}|u_n^{(1)}|^2$  for the coarse grid and  $\frac{1}{2}\Delta|u_n^{(2)}|^2$  for the coarse grid. We require that overlapping sections of the

grid have the same local energy content. In other words,

$$\frac{1}{2}|u_{2n}^{(1)}|^2 + \frac{1}{2}|u_{2n+1}^{(1)}|^2 = \frac{1}{2}\Delta|u_n^{(2)}|^2. \quad (5.6)$$

Since only one coarse grid mode is active (i.e. has a non-zero source term) for the multi-spectral DN model, we have just one such condition to satisfy, which applies to the modes

$$u_{N_1-1}^{(1)}, u_{N_1}^{(1)}, \text{ and } u_{\widehat{N_2-1}}^{(2)}. \quad (5.7)$$

The projection and prolongation operators depend on the order in which we advance the grids. We have two choices: we can advance the grids at the same time and then synchronise via projection and prolongation, or advance one at a time and project (or prolong) after we have advanced each grid separately.

### 5.D.1 Symmetric advancement

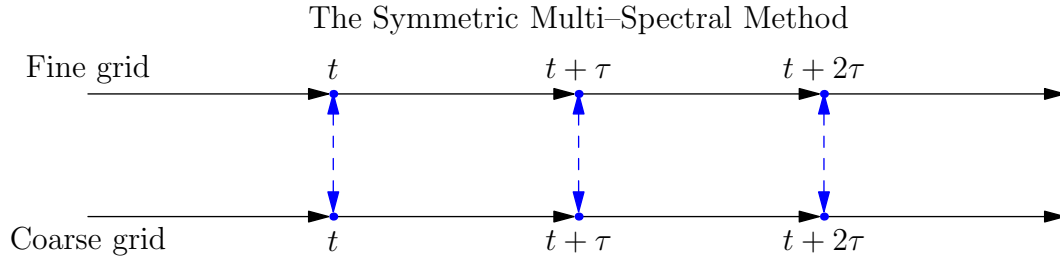


Figure 5.5: Diagram of symmetric multi-spectral method.

In the symmetric case, the projection and prolongation operators are combined into one operation. For simplicity, we consider just the triplet of interacting modes for the DN model given in (5.7). We suppose, without loss of

generality, that the triplet obeys (5.6) at the beginning of the time step. That is,

$$\frac{1}{2} \left| u(t)_{N_1-1}^{(1)} \right|^2 + \frac{1}{2} \left| u(t)_{N_1}^{(1)} \right|^2 = \frac{1}{2} \Delta \left| u(t)_{\widehat{N}_2}^{(2)} \right|^2 = E(t). \quad (5.8)$$

We advance the modes on both grids in time, sending  $t \rightarrow t + \tau$  and

$$\begin{aligned} u(t)_{N_1-1}^{(1)} &\rightarrow \tilde{u}(t + \tau)_{N_1-1}^{(1)}, \\ u(t)_{N_1}^{(1)} &\rightarrow \tilde{u}(t + \tau)_{N_1}^{(1)}, \\ u(t)_{\widehat{N}_2}^{(2)} &\rightarrow \tilde{u}(t + \tau)_{\widehat{N}_2}^{(2)}. \end{aligned} \quad (5.9)$$

The new triplet may no longer obey (5.6). Suppose

$$\begin{aligned} E_1 &= \frac{1}{2} \left| \tilde{u}(t + \tau)_{N_1-1}^{(1)} \right|^2 + \frac{1}{2} \left| \tilde{u}(t + \tau)_{N_1}^{(1)} \right|^2 \\ &\neq E_2 = \frac{1}{2} \Delta \left| \frac{1}{2} \tilde{u}(t + \tau)_{\widehat{N}_2}^{(2)} \right|^2. \end{aligned} \quad (5.10)$$

Then the change in energy of the triplet due to the coarse grid is  $E_1 - E$ , and the change in energy of the triplet due to the fine grid is  $E_2 - E$ . Over the time step  $t \rightarrow t + \tau$ , the energy content of the triplet changes from  $E$  to  $E + (E_1 - E) + (E_2 - E) = E_1 + E_2 - E$ . We can use this to prescribe the velocities, via a simultaneous projection/prolongation operator that is given

by

$$\begin{aligned}
u(t + \tau)_{N_1-1}^{(1)} &= \sqrt{\frac{E}{E_1}} \tilde{u}(t + \tau)_{N_1-1}^{(1)}, \\
u(t + \tau)_{N_1}^{(1)} &= \sqrt{\frac{E}{E_1}} \tilde{u}(t + \tau)_{N_1}^{(1)}, \\
u(t + \tau)_{\widehat{N}_2}^{(2)} &= \sqrt{\frac{E}{E_2}} \tilde{u}(t + \tau)_{\widehat{N}_2}^{(2)}.
\end{aligned} \tag{5.11}$$

This guarantees that

$$\frac{1}{2} \left| u(t + \tau)_{N_1-1}^{(1)} \right|^2 + \frac{1}{2} \left| u(t + \tau)_{N_1}^{(1)} \right|^2 = \frac{1}{2} \Delta \left| u(t + \tau)_{\widehat{N}_2}^{(2)} \right|^2 \tag{5.12}$$

Furthermore, the ratio of energies  $\frac{1}{2} \left| u(t + \tau)_{N_1-1}^{(1)} \right|^2 : \frac{1}{2} \left| u(t + \tau)_{N_1}^{(1)} \right|^2$  remains constant.

The presence of a square root in the projection/prolongation operator is of some concern, as we have no guarantee that its argument will be positive. In practise, we have never encountered a problem. Further, if it becomes negative, it may be the case that reducing the time step  $\tau$  will decrease the energy change of the system to the point that  $E(t + \tau) = E_1(t + \tau) + E_2(t + \tau) - E(t)$  will be positive. This difficulty may be avoided entirely by advancing the grids sequentially.

## 5.D.2 Sequential advancement

Advancing the grids sequentially separates the projection and prolongation operators and removes the possibility of encountering negative energy.

Again, we assume, without loss of generality, that the triplet obeys (5.6) at the beginning of the time step, i.e.  $E_1(t) = E_2(t)$ . We first advance, say,

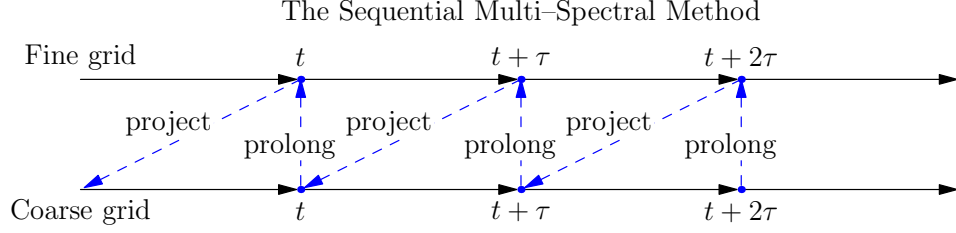


Figure 5.6: Diagram of sequential multi-spectral method.

the fine grid in time:

$$\begin{aligned}
 u(t)_{N_1-1}^{(1)} &\rightarrow \sqrt{\frac{E}{E_1}} \tilde{u}(t + \tau)_{N_1-1}^{(1)}, \\
 u(t)_{N_1}^{(1)} &\rightarrow \sqrt{\frac{E}{E_1}} \tilde{u}(t + \tau)_{N_1}^{(1)}.
 \end{aligned}
 \tag{5.13}$$

The energy of the fine grid part of the triplet is now

$$\tilde{E}_1(t + \tau) = \frac{1}{2} \left| \tilde{u}(t + \tau)_{N_1-1}^{(1)} \right|^2 + \frac{1}{2} \left| \tilde{u}(t + \tau)_{N_1}^{(1)} \right|^2.
 \tag{5.14}$$

Note that the coarse grid has not yet been advanced in time, and the grids may now disagree. We project the changes for the triplet due to the fine grid onto the coarse grid:

$$\tilde{u}(t)_{N_2}^{(2)} = \sqrt{\frac{\tilde{E}_1(t + \tau)}{E_2(t)}} u(t)_{N_2}^{(2)}.
 \tag{5.15}$$

Now, the two grids agree on the energy content of the triplet. Note that the argument of the square root involves only energy and not energy differences, so we are guaranteed that it be positive. We now advance the coarse grids in

time:

$$\tilde{u}(t)_{\widehat{N}_2}^{(2)} \rightarrow u(t + \tau)_{\widehat{N}_2}^{(2)}. \quad (5.16)$$

Again, we must restore energy balance in the triplet. We have already taken the energy transfer from the fine-grid modes to the coarse-grid modes into account via projection, so all that remains is to prolong the effect of the coarse-grid mode onto the fine-grid modes. The coarse-grid energy is now  $E_2(t + \tau) = \frac{1}{2} \Delta \left| u(t + \tau)_{\widehat{N}_2}^{(2)} \right|^2$ . Noting that the energy of the coarse-grid mode immediately before being advanced in time was  $\tilde{E}_2(t) = \tilde{E}_1(t + \tau)$ , the prolongation operator is

$$\begin{aligned} u(t + \tau)_{N_1-1}^{(1)} &= \sqrt{\frac{E_2(t + \tau)}{E_1(t + \tau)}} \tilde{u}(t + \tau)_{N_1-1}^{(1)}, \\ u(t + \tau)_{N_1}^{(1)} &= \sqrt{\frac{E_2(t + \tau)}{E_1(t + \tau)}} \tilde{u}(t + \tau)_{N_1}^{(1)}. \end{aligned} \quad (5.17)$$

At this point, the grids have both been advanced in time from  $t$  to  $t + \tau$ , and agree on the energy content of the overlapping region.

### 5.D.3 Phase propagation

Recall that the modes  $u_n^{(1)}$  and  $u_n^{(2)}$  are complex-valued. While the projection and prolongation operators guarantee that the energies of the modes in the redundant triplet agree, the phases are not accounted for. For example, the fine-grid modes may evolve to be entirely real, whereas the coarse-grid modes may remain purely imaginary. Since we require the redundant triplet of modes to at least approximately agree on the modal content of Fourier space on which

they overlap, we must modify the projection and prolongation operators to account for changes in phase. In other words we wish to set the velocity-weighted phases of the modes of the redundant triplet equal to each other, i.e. we require that

$$P_1 \doteq \frac{u_{N_1-1}^{(1)} + u_{N_1}^{(1)}}{|u_{N_1-1}^{(1)} + u_{N_1}^{(1)}|} = \frac{u_{\widehat{N_2-1}}^{(2)}}{u_{\widehat{N_2-1}}^{(2)}} \doteq P_2 \quad (5.18)$$

at the end of each time step.

Consider the case where we advance the grids symmetrically. Suppose  $P_1 = P_2$  at the beginning of the time step. We advance both grids in time from  $t$  to  $t + \tau$ , which sends

$$\begin{aligned} P_1(t) &\rightarrow P_1(t + \tau), \\ P_2(t) &\rightarrow P_2(t + \tau). \end{aligned} \quad (5.19)$$

The change in phases over the time step are  $P_1(t+\tau)/P_1(t)$  and  $P_2(t+\tau)/P_2(t)$ . There is some danger that a denominator will become zero, but, again, this has never been observed to occur. If it does occur, one should replace the change in phase by a random phase, which prevents the introduction of phase-bias into the system.

We require all modes in the redundant triplet to change by

$$P \doteq \frac{P_1(t + \tau)}{P_1(t)} \times \frac{P_2(t + \tau)}{P_2(t)}. \quad (5.20)$$

This can be incorporated into the projection/prolongation operator given by (5.11),

which becomes

$$\begin{aligned}
u(t + \tau)_{N_1-1}^{(1)} &= P \sqrt{\frac{E}{E_1}} \tilde{u}(t + \tau)_{N_1-1}^{(1)}, \\
u(t + \tau)_{N_1}^{(1)} &= P \sqrt{\frac{E}{E_1}} \tilde{u}(t + \tau)_{N_1}^{(1)}, \\
u(t + \tau)_{N_2}^{(2)} &= P \sqrt{\frac{E}{E_2}} \tilde{u}(t + \tau)_{N_2}^{(2)}.
\end{aligned} \tag{5.21}$$

In the case where we advance the grids sequentially, the projection operator in (5.15) becomes

$$\tilde{u}(t)_{N_2}^{(2)} = \frac{P_1(t + \tau)}{P_1(t)} \sqrt{\tilde{E}_1(t + \tau)/E_2(t)} u(t)_{N_2}^{(2)}, \tag{5.22}$$

and the prolongation operator given by (5.17) becomes

$$\begin{aligned}
u(t + \tau)_{N_1-1}^{(1)} &= \frac{P_2(t + \tau)}{P_2(t)} \sqrt{\frac{E_2(t + \tau)}{E_1(t + \tau)}} \tilde{u}(t + \tau)_{N_1-1}^{(1)}, \\
u(t + \tau)_{N_1}^{(1)} &= \frac{P_2(t + \tau)}{P_2(t)} \sqrt{\frac{E_2(t + \tau)}{E_1(t + \tau)}} \tilde{u}(t + \tau)_{N_1}^{(1)}.
\end{aligned} \tag{5.23}$$

We expect that the addition of phase-changes to the projection and prolongation operators will be particularly important for Navier–Stokes turbulence where coherent structures play an important role.

## 5.E Application of spectral reduction

While we have established how to simulate a system on a variable-resolution grid in Fourier-space using two grids, we must now ensure that it is the same system that we are approximating on both grids. In particular, we must

determine the effect of binning modes on the governing equation. We use the method of spectral reduction (Chapter 4) to predict how binning will effect the governing equation.

The approximation

$$u_n^{(2)} = \frac{1}{\Delta} \left( u_{2n}^{(2)} + u_{2n+1}^{(2)} \right) \quad (5.24)$$

is equivalent to setting  $\sigma_n^{(0)} \equiv 1$ . Setting  $u_n^{(2)} = u_{2n}^{(2)} = u_{2n+1}^{(2)}$  closes the equations. With the use of the multi-spectral method, this is equivalent to the assumption that the phases of the adjacent modes  $u_{2n}^{(2)}$  and  $u_{2n+1}^{(2)}$  are correlated. However, this is not the case for the DN model, where adjacent modes are completely uncorrelated. In particular, if we take the sum of adjacent modes, we expect that

$$\begin{aligned} \left\langle |u_{2n}^{(2)} + u_{2n+1}^{(2)}|^2 \right\rangle &= \left\langle |u_{2n}^{(2)}|^2 \right\rangle + 2 \left\langle \cancel{u_{2n}^{(2)} u_{2n+1}^{(2)*}} \right\rangle \xrightarrow{0} \left\langle |u_{2n+1}^{(2)}|^2 \right\rangle \\ &= \left\langle |u_{2n}^{(2)}|^2 \right\rangle + \left\langle |u_{2n+1}^{(2)}|^2 \right\rangle. \end{aligned} \quad (5.25)$$

Because of this, we use the approximation

$$u_n^{(2)} = \frac{1}{\sqrt{\Delta}} \left( u_{2n}^{(2)} + u_{2n+1}^{(2)} \right). \quad (5.26)$$

Using (5.26), we can use spectral reduction to determine the coefficients for grid  $\ell + 1$  in terms of the coefficients for grid  $\ell$ :

$$a^{(\ell+1)} = \frac{a^{(\ell)}}{\sqrt{2}}, \quad b^{(\ell+1)} = \frac{b^{(\ell)}}{\sqrt{2}}, \quad \text{and} \quad \nu^{(\ell+1)} = \nu^{(\ell)} \frac{1 + \lambda^{(\ell)2}}{\sqrt{2}}. \quad (5.27)$$

## 5.F Extension to many grids

We can extend the multi-spectral method to a hierarchy of grids to further reduce the number of modes in the system. In the sequential case, it is simple to extend the method, as shown in Fig. 5.7. With  $N$  grids, one simply advances the finest grid in time, projects onto the next-finest grid, advances that grid in time, projects onto the finest grid after that, and continues down until one has reached the coarsest grid. One can then prolong from the coarsest grid to the next coarsest grid, and so on, until one prolongs from the second-finest grid onto the finest grid. At this point, all grids have been advanced in time and synchronised by the projection and prolongation operators.

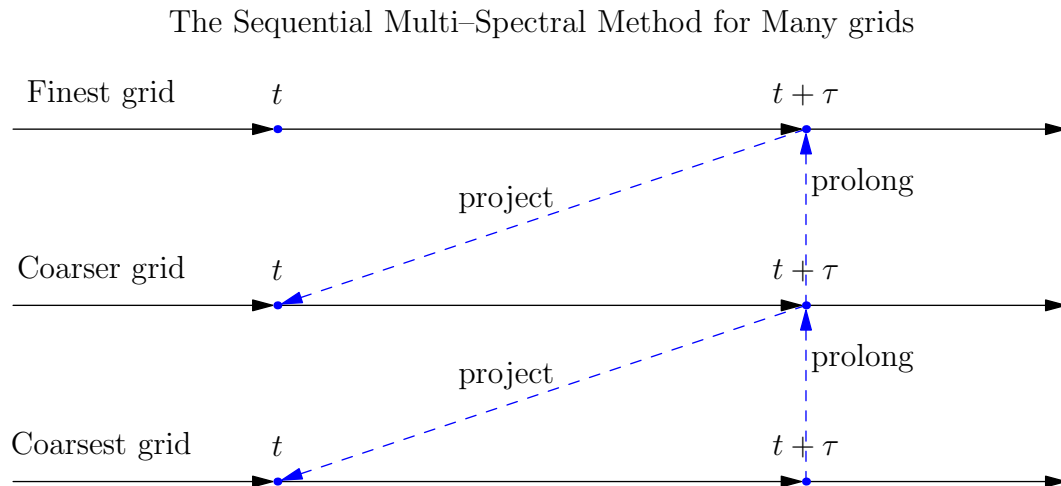


Figure 5.7: Sequential time advancement with many grids.

## 5.G Properties of the multi-spectral method

The advantage of the multi-spectral method is that we can solve a system in Fourier space using a grid with resolution that varies with wavenumber. Unlike

the method of spectral reduction, we do not need to rescale time in order to reach equipartition, so the low-resolution system is no stiffer than the original system.

We can arbitrarily set the fraction of the system that is at high or low resolution. This allows us to determine the effect of our approximation on the behaviour of the system relative to the full-resolution system.

Since the projection and prolongation operators were created with energy conservation in mind, the entire system conserves energy so long as the spectrally reduced model conserves energy on each grid independently.

We can use a radix-two multi-spectral method on a system whenever the number of modes in the system,  $N$ , is divisible by two. We can extend this to a hierarchy of  $n$  grids if  $2^{n-1}$  divides  $N$ . If we assume that all the grids have the same number of modes, then each grid has  $N/2^{n-1}$  modes, and there are  $nN/2^{n-1}$  modes total. This is a significant savings in memory, as can be seen in Fig. 5.8. For example, using 16 grids reduces the number of modes by a factor of 2048. Using just two grids provides no savings whatsoever, unless we extend the coarse grid to cover more than half the original system. If the model has localised interactions (e.g. the DN model and the GOY model), many of the modes on a grid are inactive on all but the finest grid, and can therefore be eliminated.

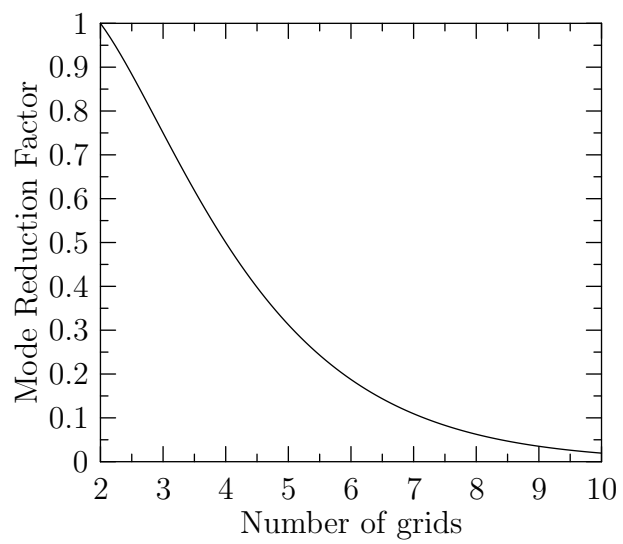


Figure 5.8: The ratio of the number of modes in a spectrally reduced system to the number of modes in the original system.

# Chapter 6

## Simulations and Results

*In which we demonstrate various results of our technique.*

All simulations were done using the DN model. It is an ideal test-bed for the multi-spectral method because of its simplicity and the fact that the form of the equation is invariant under spectral reduction. We used the Triad C++ initial-value problem integrator [Bowman 2004], and we made use of the exponential [Bowman *et al.* 2006], [Bowman 2006] and conservative [Shadwick *et al.* 1999], [Bowman *et al.* 1997], [Kotovych & Bowman 2002], [Shadwick *et al.* 2001] numerical integration schemes contained therein whenever we could.

### 6.A Inviscid turbulence

In Chapter 3 we established several results for inviscid, unforced turbulence. We expect that the energy spectrum  $E(k)$  of the DN model should scale like  $k^{-1}$  once the system has reached a steady state.

Before we show the results of the multi-spectral method, it will be insightful to explore an alternative approach, in which one simply adds the source term

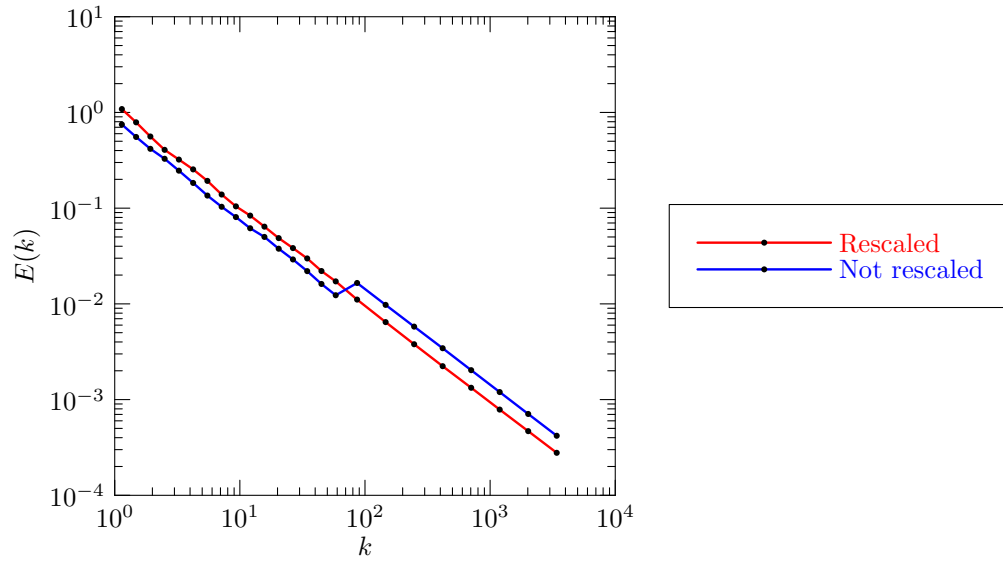


Figure 6.1:  $E(k)$  vs.  $k$  for inviscid unforced turbulence with two grids and source transfer.

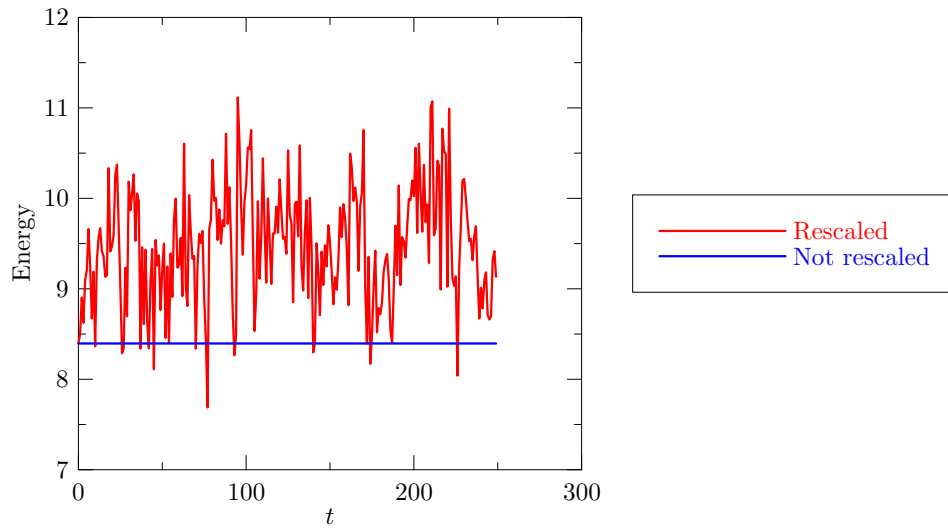


Figure 6.2: Energy vs. time for inviscid unforced turbulence with two grids and source transfer.

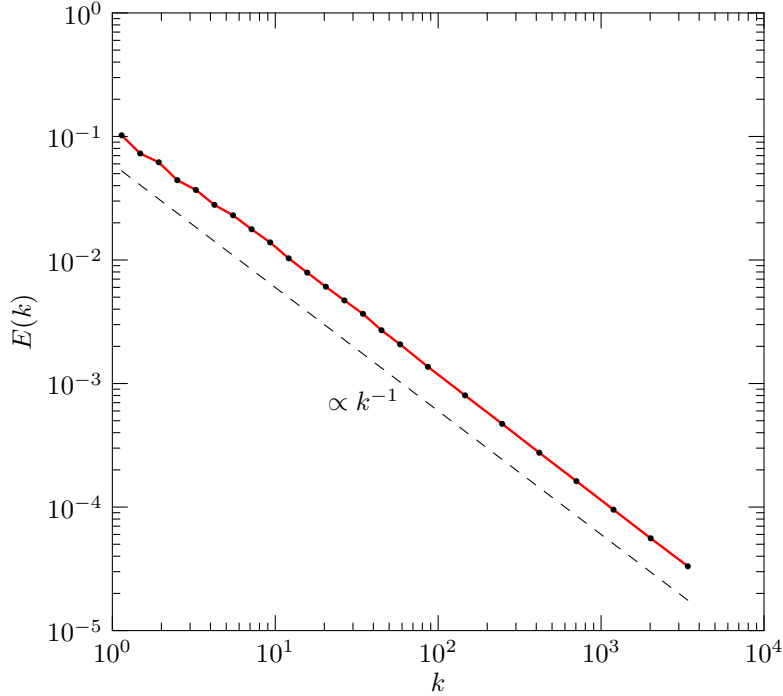


Figure 6.3:  $E(k)$  vs.  $k$  for inviscid unforced turbulence with two grids with projection/prolongation.

for the coarse mode of the redundant triplet to the fine modes. In that the resulting computational problem would be more straightforward, this method is preferable to the multi-spectral method. However, transferring the source term between grids is equivalent to spectral reduction with variable bin sizes, which does not correctly reproduce the equipartition spectrum. As can be seen in Fig. 6.1, transferring the source term between grids produces an anomalous discontinuity in the spectrum. While this may be fixed by rescaling time by the relative bin sizes, this breaks energy conservation, as demonstrated in Fig 6.2.

Using the multi-spectral method, we are able to reproduce the equipartition spectrum faithfully without resorting to rescaling time (Fig. 6.3.). Such a system conserves energy (up to machine precision) and is less stiff than a system in which time has been rescaled by the relative bin sizes. In fact,

the multi-spectral method is able to reproduce the equipartition spectrum for inviscid unforced turbulence even if time has been rescaled on each grid by an arbitrary factor.

## 6.B Forced-dissipative turbulence

In Chapter 2 we established results for forced-dissipative turbulence where energy is injected at the large scales. We expect such systems to exhibit an energy spectrum of  $E(k) \sim k^{-5/3}$  at intermediate wavenumbers, and for energy to fall off rapidly at wavenumbers greater than the dissipation wavenumber. Under suitable conditions, the multi-spectral method is able to reproduce these spectra. Forced-dissipative turbulence appears to be more sensitive to the choice of projection and prolongation operators than near-equilibrium systems (those approaching equipartition).

In the absence of phase communication, the transfer of energy is slightly diminished at the interface between the grids, and the effect of this on the energy spectrum is shown in Fig. 6.4. While the effect of phase-communication is slight for shell models, it is important for two- or three-dimensional Navier–Stokes turbulence where phase is instrumental to the preservation of coherent structures.

The assumption of adjacent-mode correlation also has a significant effect on the forced-dissipative spectrum. Fig. (6.5) shows the effect of assumptions

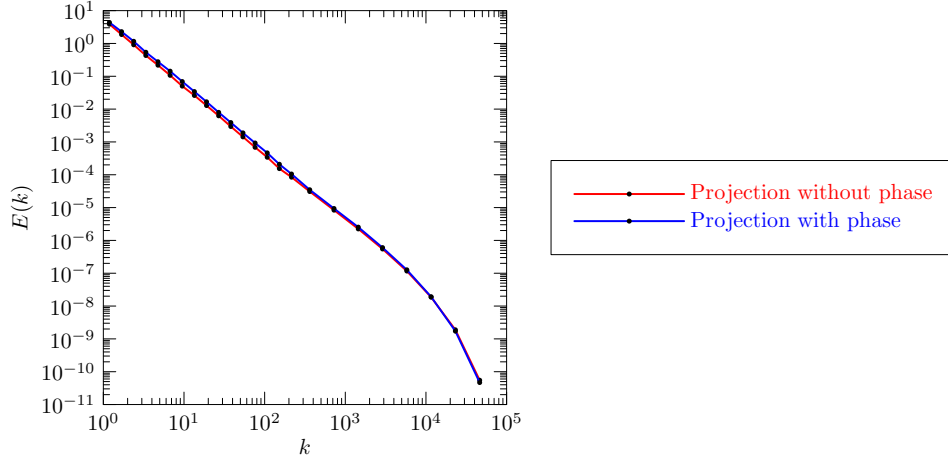


Figure 6.4:  $E(k)$  vs.  $k$  for forced-dissipative DN turbulence showing the effect of phase communication.

about how modes are correlated. The assumptions we use are:

$$u_n^{(\ell+1)} \approx \frac{u_{2n}^{(\ell)} + u_{2n+1}^{(\ell)}}{2}, \quad (6.1)$$

$$u_n^{(2)} \approx \frac{u_{2n}^{(\ell)} + u_{2n+1}^{(\ell)}}{\sqrt{2}}, \quad (6.2)$$

$$u_n^{(2)} \approx u_{2n}^{(\ell)} + u_{2n+1}^{(\ell)}. \quad (6.3)$$

Here, (6.1) follows from the assumption that adjacent modes are correlated, while (6.2) follows from the assumption that adjacent modes are uncorrelated, and (6.3) is put in for the sake of comparison. These assumptions amount to various rescalings of time between grids, which effects the forced-dissipative spectrum but not the equipartition spectrum.

If we assume that adjacent modes are correlated (6.1) then the interaction coefficients on the coarse grid are too small, i.e. the time scales are large. The effect on the spectrum is to slow energy transfer between grids, which produces an anomalous energy bottleneck at the grid boundary, which increased

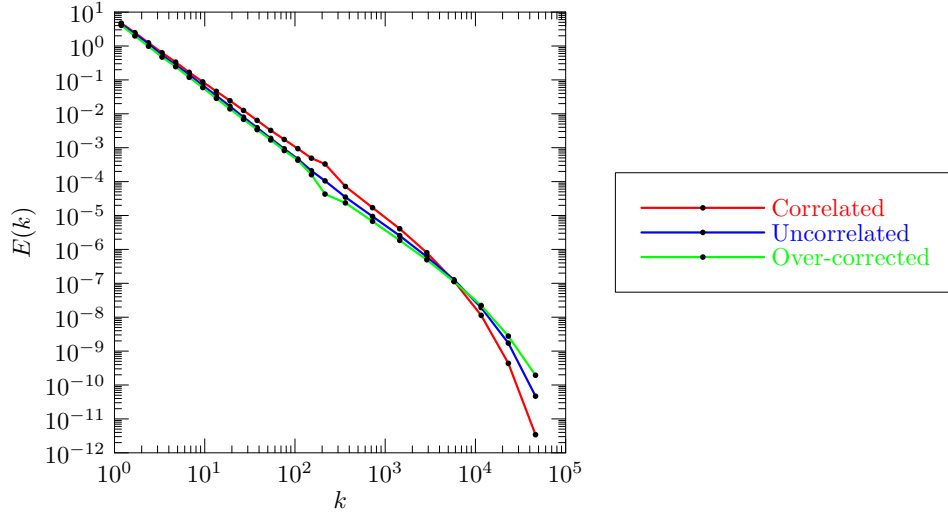


Figure 6.5:  $E(k)$  vs.  $k$  for forced-dissipative DN turbulence showing the effect of assumptions of adjacent-mode correlation given by (6.1), (6.2), and (6.3).

the energy of the boundary mode in the fine grid. Energy is depressed at high wavenumbers because of the bottleneck at the grid boundary. If we do not change the interaction coefficients at all, using (6.3), the coarse grid has larger interaction coefficients, which increases the energy transfer between grids, creating an anomalous drop in energy at the grid boundary. Similarly, energy at the small scales is anomalously elevated. Using the assumption that adjacent modes are uncorrelated (6.2), normal inter-grid energy transfer is established, resulting in a smooth spectrum at the grid boundaries and normal energy levels at the small scales. This effect is very pronounced for simulations with more than two grids, where the repeated application of the method of spectral reduction can change time scales significantly.

## 6.C Simulations with several grids

We can easily extend our method to a hierarchy of grids. This significantly reduces the number of modes while still covering the same region of Fourier space. We show comparisons of simulations using two, three, four, and five grids. The multi-spectral method is able to reproduce both inviscid spectra (Fig. (6.6)) and the spectra for forced-dissipative turbulence (Figs. 6.7, 6.8, 6.9, and 6.10). These simulations were made using sequential grid advancement, phase communication, and the assumption that adjacent modes are uncorrelated. To better compare simulations, we bin the modes for one-grid simulations to match the distribution of modes in a many-grid simulation. Even the simulation with five grids (Fig. 6.10), with only three active modes on the coarse grids, still closely reproduces the spectra predicted by the full-resolution simulation.

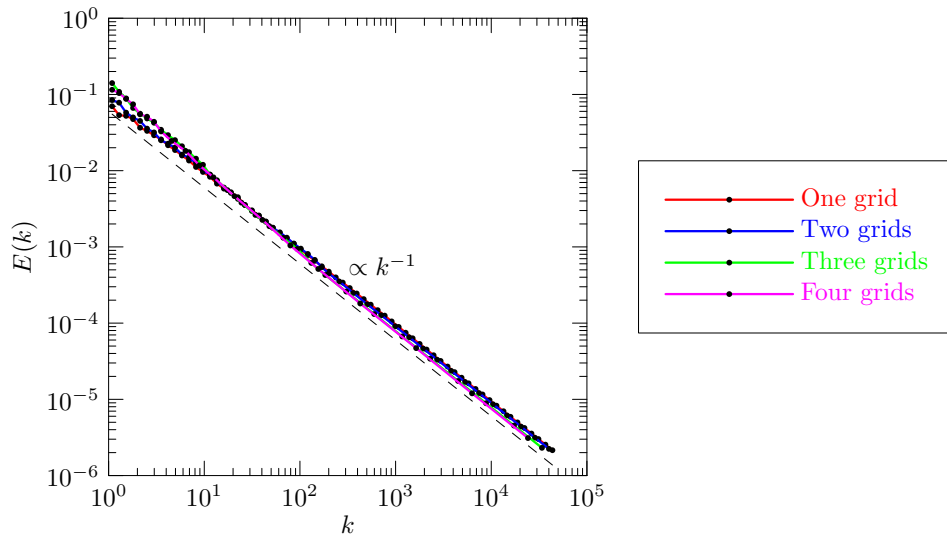


Figure 6.6: Multi-spectral simulations of inviscid turbulence with one, two, three, or four grids.

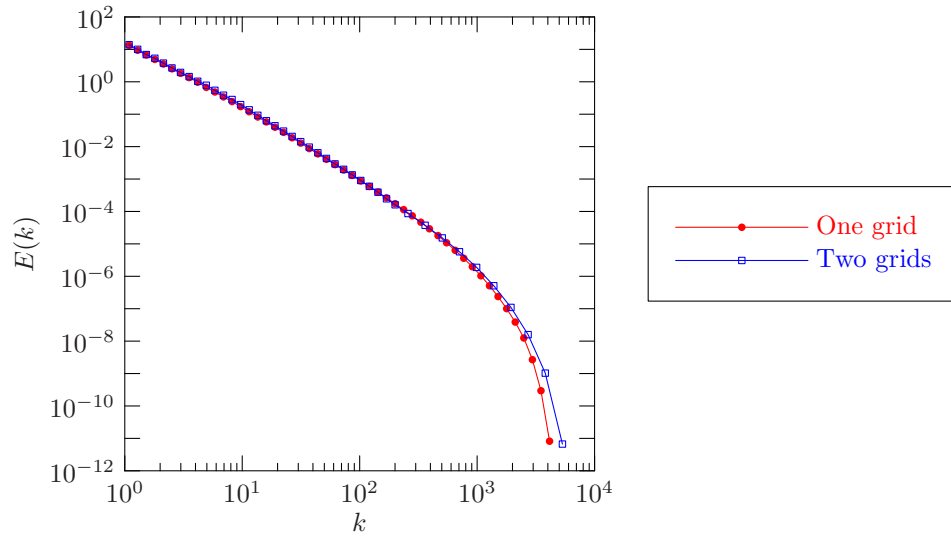


Figure 6.7: Multi-spectral simulation of forced-dissipative turbulence with two grids.

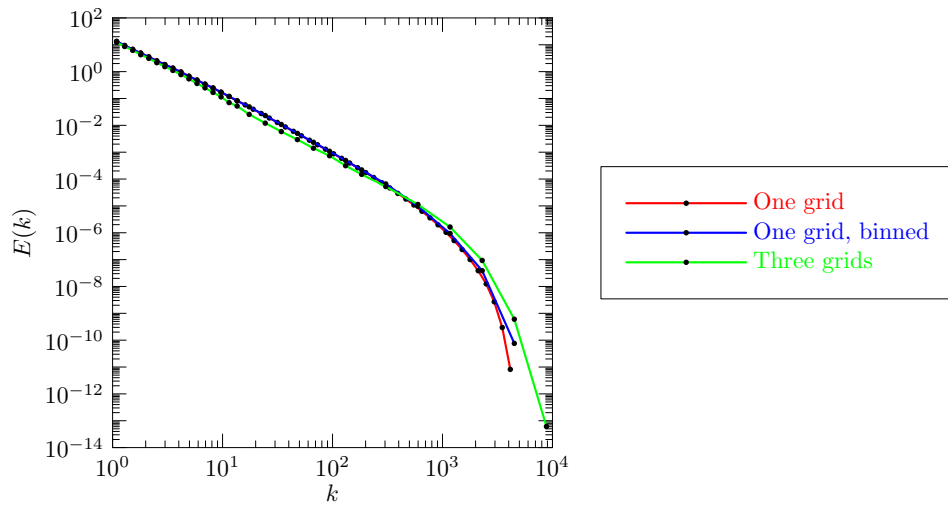


Figure 6.8: Multi-spectral simulation of forced-dissipative turbulence with three grids.

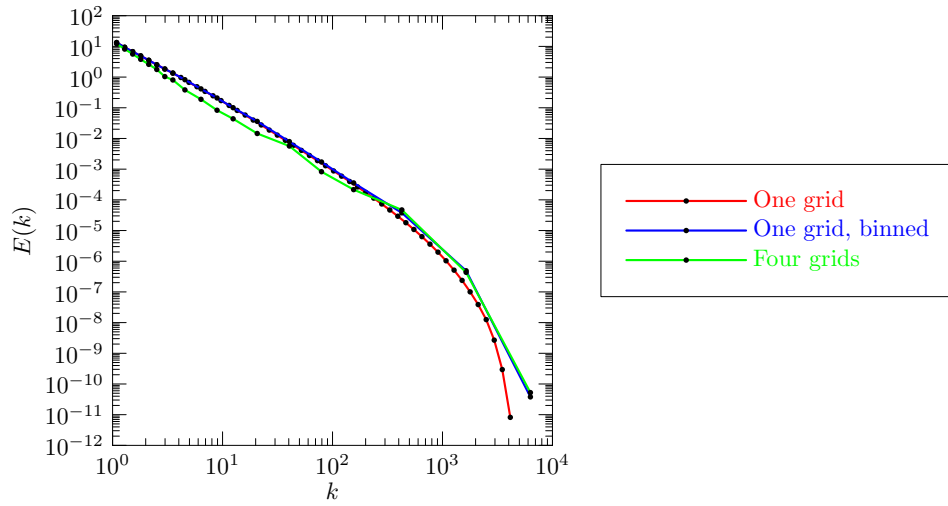


Figure 6.9: Multi-spectral simulation of forced-dissipative turbulence with four grids.

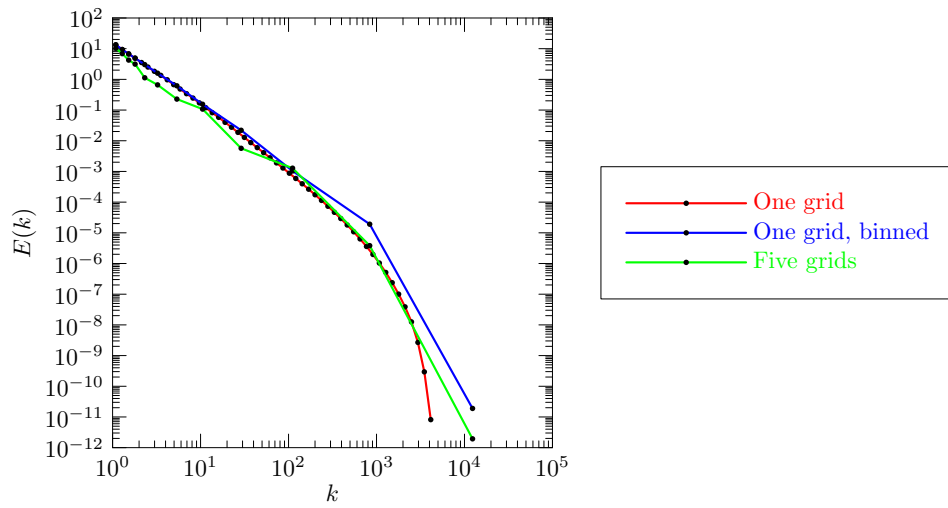


Figure 6.10: Multi-spectral simulation of forced-dissipative turbulence with five grids.

# Chapter 7

## Conclusions

*In which we describe possible applications of our technique and discuss further research.*

The multi-spectral method is able to reproduce the behaviour of high-resolution systems, but uses dramatically fewer modes. We were able to reproduce energy spectra of the DN model correctly using two to five grids, limited only by the original resolution of the model.

### 7.A Future work

The multi-spectral method has been studied for shell models of turbulence only. Shell models have very few intermodal interactions when compared with the Navier–Stokes equation. The application of a multi-spectral method to Navier–Stokes turbulence may be an easier problem than the application of a multi-spectral method to a shell model of turbulence since the Navier–Stokes turbulence has more inter-modal interactions that cross grid boundaries. This may prevent a bottleneck of energy transfer at grid boundaries, meaning that

the Navier–Stokes equation may be less sensitive to the assumptions in the method of spectral reduction that determine how one should rescale interaction coefficients from one grid to another. The multi-spectral method might yield an even more significant decimation on Navier–Stokes turbulence due to the fact that the binning factor will grow like  $2^D$  where  $D$  is the dimension of the turbulence.

However, complications will most certainly arise. In particular, we expect that the projection and prolongation operators will have to be modified to accommodate geometric effects. In the case of two-dimensional turbulence, they will also have to conserve enstrophy, which may place a severe constraint on both the choice of projection and prolongation operators and the relative geometry of the fine and coarse grids.

In addition to such theoretical concerns, we would like to apply the method of spectral reduction to turbulence of physical interest. Our method was formulated in Fourier space, with the assumption of periodic boundary conditions. While this is unphysical, it may be a good approximation for the behaviour of turbulence at the small scales. Ideally, we would like to be able to use spectral reduction as a sub-grid model for turbulence, approximating the behaviour at the small scales. In this fashion, we may be able to apply spectral reduction to inhomogeneous turbulence, which is believed to become homogeneous at the small scales.

One problem that spectral reduction does not address is the stiffness of the resulting system, which inherits the wide range of time scales from the original problem. There may be hope; perhaps using different integration methods on different grids could address this problem. For example, a lower-order conservative Runge–Kutta [Bowman *et al.* 1997] scheme on the fine grid, where

energy is injected but not dissipated, and a higher-order exponential Runge–Kutta scheme [Bowman *et al.* 2006], [Bowman 2006] on the coarse grid, where the linear term often imposes an upper bound on the time step.

## 7.B Applications

Immediately, the method of spectral reduction can be used to better understand the behaviour of shell models of turbulence at high Reynolds numbers. For instance, the dependence of the dissipation wavenumber on  $\nu$ , the coefficient of linear viscosity, or studies of intermittent behaviour could be fruitful avenues of research.

The multi-spectral method could potentially be useful for simulating weather and climate changes. Further, we may be able to apply a multi-spectral reduction to magnetohydrodynamical systems, where the Navier–Stokes equation is coupled to Maxwell’s equations. In particular, there is a need for high-resolution simulations of plasma turbulence simulations to understand energy transport in Tokamak fusion reactors. We hope that we will be able to apply the multi-spectral method not only to the equations of turbulence, but to a wide variety of physical systems represented by systems of partial differential equations.

# Bibliography

- [Ames 1977] W. Ames, *Numerical Methods for Partial Differential Equations*, Academic Press, San Diego, CA, 1977.
- [Basu & Porté-Agel 2005] S. Basu & F. Porté-Agel, 2005.
- [Batchelor 1969] G. K. Batchelor, *Phys. Fluids*, **12 II**:233, 1969.
- [Bell & Nelkin 1977] T. Bell & M. Nelkin, *Phys. Fluids*, **20**:345, 1977.
- [Benzi *et al.* 2004] R. Benzi, L. Biferale, & M. Sbragaglia, 2004.
- [Biferale *et al.* 1995] L. Biferale, A. Lambert, R. Lima, & G. Paladin, *Physica D*, **80**:105, 1995.
- [Biferale 2003] L. Biferale, *Annu. Rev. Fluid Mech.*, **35**:441, 2003.
- [Boffetta & Romano 2002] G. Boffetta & G. P. Romano, *Physics of Fluids*, **14**:3453, 2002.
- [Bohr *et al.* 1998] T. Bohr, M. H. Jensen, G. Paladin, & A. Vulpiani, *Dynamical Systems Approach to Turbulence*, Cambridge Univ. Press, Cambridge, 1998.
- [Bowman & Krommes 1997] J. C. Bowman & J. A. Krommes, *Phys. Plasmas*, **4**:3895, 1997.
- [Bowman *et al.* 1993] J. C. Bowman, J. A. Krommes, & M. Ottaviani, *Phys. Fluids B*, **5**:3558, 1993.
- [Bowman *et al.* 1996] J. C. Bowman, B. A. Shadwick, & P. J. Morrison, “Spectral reduction for two-dimensional turbulence,” in *Transport, Chaos, and Plasma Physics 2*, edited by S. Benkadda, F. Doveil, &

- Y. Elskens, pp. 58–73, New York, 1996, Institute Méditerranéen de Technologie (Marseille, 1995), World Scientific.
- [Bowman *et al.* 1997] J. C. Bowman, B. A. Shadwick, & P. J. Morrison, “Exactly conservative integrators,” in *15th IMACS World Congress on Scientific Computation, Modelling and Applied Mathematics*, edited by A. Sydow, volume 2, pp. 595–600, Berlin, 1997, Wissenschaft & Technik.
- [Bowman *et al.* 1999] J. C. Bowman, B. A. Shadwick, & P. J. Morrison, Phys. Rev. Lett., **83**:5491, 1999.
- [Bowman *et al.* 2001] J. C. Bowman, B. A. Shadwick, & P. J. Morrison, “Numerical challenges for turbulence computation: Statistical equipartition and the method of spectral reduction,” in *Scientific Computing and Applications*, edited by P. Mineev, Y. S. Wong, & Y. Lin, volume 7 of *Advances in Computation: Theory and Practice*, pp. 171–178, Huntington, New York, 2001, Nova Science Publishers.
- [Bowman *et al.* 2006] J. C. Bowman, C. R. Doering, B. Eckhardt, J. Davoudi, M. Roberts, & J. Schumacher, Physica D, **218**:1, 2006.
- [Bowman 1992] J. C. Bowman, *Realizable Markovian Statistical Closures: General Theory and Application to Drift-Wave Turbulence*, Ph.D. thesis, Princeton University, Princeton NJ, USA, 1992.
- [Bowman 1996] J. C. Bowman, J. Fluid Mech., **306**:167, 1996.
- [Bowman 2004] J. C. Bowman, *Triad*: an object-oriented C++ package for integrating initial value problems. <http://www.math.ualberta.ca/~bowman>, 2004.
- [Bowman 2006] J. C. Bowman, Canadian Applied Mathematics Quarterly, **14**:223, 2006.
- [Bramble 1993] J. H. Bramble, *Multigrid Methods*, Longman Scientific and Technical, London, 1993.

- [Briggs 1987] W. L. Briggs, *A Multigrid Tutorial*, SIAM, Philadelphia, 1987.
- [de Kármán & Howarth 1937] T. de Kármán & T. Howarth, 1937.
- [Desnyansky & Novikov 1974] V. N. Desnyansky & E. A. Novikov, *Prikl. Mat. Mekh.*, **38**:507, 1974.
- [Dubos 2003] T. Dubos, 2003.
- [Eckhardt 2004] B. Eckhardt, private communication, 2004.
- [Farge 2006] M. Farge, private communication, 2006.
- [Fjørtoft 1953] R. Fjørtoft, *Tellus*, **5**:225, 1953.
- [Frisch 1995] U. Frisch, *Turbulence: The Legacy of A.N.Kolmogorov*, Cambridge University Press, 1995.
- [Gledzer 1973] E. B. Gledzer, *Sov. Phys. Dokl.*, **18**:216, 1973.
- [Gottlieb & Orszag 1977] D. Gottlieb & S. A. Orszag, *Numerical Analysis of Spectral Methods: Theory and Applications*, Society for Industrial and Applied Mathematics, Philadelphia, 1977.
- [Hackbusch 1985] W. Hackbusch, *Multi-Grid Methods and Applications*, Series in Computational Mathematics, Springer, New York, 1985.
- [Herweijer & van de Water 1995] J. Herweijer & W. van de Water, *Phys. Rev. Lett.*, **74**:4651, 1995.
- [Kadanoff *et al.* 1995] L. P. Kadanoff, D. Lohse, J. Wang, & R. Benzi, *Phys. Fluids*, **7**:617, 1995.
- [Kolmogorov 1941a] A. Kolmogorov, *Dokl. Akad. Nauk SSSR*, **30**:301, 1941, Reprinted in *Proc. R. Soc. Lond. A434*, 9–13,1991.
- [Kolmogorov 1941b] A. Kolmogorov, *Dokl. Akad. Nauk SSSR*, **32**:16, 1941, Reprinted in *Proc. R. Soc. Lond. A434*, 15–17,1991.
- [Kotovych & Bowman 2002] O. Kotovych & J. C. Bowman, *J. Phys. A.: Math. Gen.*, **35**:7849, 2002.

- [Kraichnan 1967] R. H. Kraichnan, Phys. Fluids, **10**:1417, 1967.
- [Kraichnan 1971] R. H. Kraichnan, J. Fluid Mech., **47**:513, 1971.
- [Kraichnan 1972] R. H. Kraichnan, J. Fluid Mech., **56**:287, 1972.
- [Kraichnan 1975] R. H. Kraichnan, J. Fluid Mech., **67**:155, 1975.
- [L'vov *et al.* 1998] V. S. L'vov, E. Podivilov, A. Pomyalov, I. Procaccia, & D. Vandembroucq, Phys. Rev. E, **58**:1811, 1998.
- [McWilliams 1984] J. C. McWilliams, J. Fluid Mech., **146**:21, 1984.
- [Melander & Fabijonas 2006] M. Melander & B. Fabijonas, 2006.
- [Monin & Yaglom 1965] A. S. Monin & A. M. Yaglom, *Statistical Fluid Mechanics; Mechanics of Turbulence*, MIT Press, Cambridge, Massachusetts, 1965, English translation published in 1971, edited by John L. Lumley.
- [Morrison 1998] P. J. Morrison, Rev. Mod. Phys., **70**:467, 1998.
- [Nelkin 2001] M. Nelkin, 2001.
- [Novikov 1964] E. A. Novikov, J. Exptl. Theoret. Phys. (U.S.S.R), **47**:1919, 1964.
- [Orszag 1970] S. A. Orszag, J. Fluid Mech., **41**:363, 1970.
- [Orszag 1977] S. A. Orszag, "Lectures on the statistical theory of turbulence," in *Fluid Dynamics*, edited by R. Balian & J.-L. Peube, pp. 235–373, Gordon and Breach, London, 1977, (summer school lectures given at Grenoble University, 1973).
- [Piomelli *et al.* 1991] U. Piomelli, W. Cabot, P. Moin, & S. Lee, Phys. Fluids A, **3**:1766, 1991.
- [Shadwick *et al.* 1999] B. A. Shadwick, J. C. Bowman, & P. J. Morrison, SIAM J. Appl. Math., **59**:1112, 1999.

- [Shadwick *et al.* 2001] B. A. Shadwick, W. F. Buell, & J. C. Bowman, “Structure preserving integration algorithms,” in *Scientific Computing and Applications*, edited by P. Mineev, Y. S. Wong, & Y. Lin, volume 7 of *Advances in Computation: Theory and Practice*, pp. 247–255, New York, 2001, Nova Science Publishers.
- [Tran & Bowman 2003] C. V. Tran & J. C. Bowman, *Physica D*, **176**:242, 2003.
- [Tran & Shepherd 2002] C. V. Tran & T. G. Shepherd, *Physica D*, **165**:199, 2002.
- [Yahalom 1994] A. Yahalom, Helicity conservation via the Noether theorem, 1994.
- [Yamada & Ohkitani 1987] M. Yamada & K. Ohkitani, *J. Phys. Soc. Jap.*, **56**:4210, 1987.

# Index

- $\doteq$ , 3
- back-scatter, 52
- bottlenecks, 52
- Casimir invariants, 7
- coarse grid, 56
- continuity equation, 2
- coupling coefficients, 10
- eddy-damped quasinormal Markovian, 53
- energy density, 11
- energy spectrum, 11
- enstrophy, 7
- Eulerian derivative, 2
- fine grid, 56
- flux, 15
- four-fifths law, 20
- Gibbs distribution, 36
- Gibbs H theorem, 35
- hyperviscosity, 52
- incompressible, 2
- inertial range, 18
- Lagrangian derivative, 2
- laminar, 5
- Liouville theorem, 35
- multi-spectral method, 1, 55
- Noether's theorem, 3
- phase space, 34
- pseudo-spectral, 4
- quasinormal, 53
- realisable Markovian closure, 53
- realisable test field model, 53
- redundant, 56
- Reynolds number, 5
- second-order intermittency correction, 31
- spectral reduction, 41
- statistical closure, 53
- test field model, 53
- visible modes, 57
- vorticity, 6